

Entangling distant resonant exchange qubits via circuit quantum electrodynamics

V. Srinivasa,^{1,2,*} J. M. Taylor,^{3,4,5} and C. Tahan¹

¹*Laboratory for Physical Sciences, College Park, Maryland 20740, USA*

²*Department of Physics, University of Maryland, College Park, Maryland 20742, USA*

³*Joint Quantum Institute, University of Maryland, College Park, Maryland 20742, USA*

⁴*Joint Center for Quantum Information and Computer Science,
University of Maryland, College Park, Maryland 20742, USA*

⁵*National Institute of Standards and Technology, Gaithersburg, Maryland, 20899, USA*

We investigate a hybrid quantum system consisting of spatially separated resonant exchange qubits, defined in three-electron semiconductor triple quantum dots, that are coupled via a superconducting transmission line resonator. Drawing on methods from circuit quantum electrodynamics and Hartmann-Hahn double resonance techniques, we analyze three specific approaches for implementing resonator-mediated two-qubit entangling gates in both dispersive and resonant regimes of interaction. We calculate entangling gate fidelities as well as the rate of relaxation via phonons for resonant exchange qubits in silicon triple dots and show that such an implementation is particularly well-suited to achieving the strong coupling regime. Our approach combines the favorable coherence properties of encoded spin qubits in silicon with the rapid and robust long-range entanglement provided by circuit QED systems.

I. INTRODUCTION

The simultaneous realization of coherent local control of quantum bits (qubits) and robust long-range interactions for entangling distant qubits represents a fundamental goal in many proposed implementations of quantum information processing.^{1,2} Hybrid approaches may prove particularly advantageous for achieving this goal, as they enable the optimal properties of multiple physically distinct quantum systems to be combined.³

Electron spin qubits in semiconductor quantum dots promise protection from environmental decoherence and potential scalability to larger systems.^{3–6} An alternative to the challenges of coherently controlling single electron spins via, e.g., highly localized magnetic fields,⁷ spin-orbit coupling,^{8,9} or spin-position coupling via magnetic field gradients^{10,11} is provided by the encoding of single logical qubits in multiple electron spins.^{5,12–18} Within systems of two or more coupled quantum dots, such an encoding effectively translates magnetic field control to electric field control, providing a means of rapidly manipulating individual qubits, while allowing for operation within decoherence-free subspaces that protect against collective decoherence and leakage errors.¹⁹

Three-electron spin qubits enable universal manipulation to be achieved via electric field control of exchange interactions alone.^{14–18,20–23} However, the electrostatic origin of exchange renders these spin qubits susceptible to charge noise. The particular form of the exchange-only qubit known as the resonant exchange (RX) qubit enables high-frequency operation via resonant microwave driving of the exchange at a “sweet spot,” where a large exchange energy gap suppresses the sensitivity of the qubit to low-frequency charge noise.^{17,18,24–26} Thus, the RX qubit represents a semiconductor qubit similar to the transmon superconducting qubit^{27,28} that additionally possesses the protection intrinsic to spin qubits.^{3,6}

A key element of a scalable quantum information pro-

cessor based on multielectron spin qubits is the implementation of long-range entangling gates. The exchange interaction can be used to perform rapid, protected gates between neighboring exchange-only qubits;^{14,29–33} however, the range of the interaction is limited by its dependence on the overlap of the wave functions of the electrons participating in the coupling, which decreases exponentially with the separation between electrons.^{19,34} Longer-range coupling is possible via the Coulomb interaction and can be used to carry out entangling gates between adjacent capacitively coupled exchange-only qubits^{18,35,36} without the leakage intrinsic to two-qubit exchange gates.^{14,29,30,32,33,37} The range of exchange-based interactions can be extended via spin chains,^{38,39} while that of capacitive interactions can be extended via floating metal gates.⁴⁰ In the context of a modular quantum computer architecture,^{5,41} these schemes provide potential methods of coupling spatially separated spin qubits within a single module.

In order to enable full scalability and modularity within a quantum information processing device, however, a rapid and robust interaction between qubits within different modules that are separated by macroscopic distances is highly desirable.^{5,41} For superconducting qubits, such an interaction can be realized within the approach of circuit quantum electrodynamics (QED), where qubits separated by distances of up to the order of centimeters are coupled capacitively to the microwave field of a superconducting transmission line resonator.^{42–48} An analogous approach has been investigated for hybrid solid-state quantum systems consisting of semiconductor charge^{49–54} or spin^{49,55–61} qubits coupled to a superconducting resonator. The potentially longer coherence times possible for spin qubits, particularly in silicon,^{23,62–67} in comparison to superconducting qubits and quantum dot charge qubits are advantageous for achieving the strong coupling regime, in which the interaction rate exceeds both the qubit and cavity decay

rates.^{42,49}

Here, we consider two RX qubits coupled via the fundamental mode of a superconducting transmission line resonator as a potential building block for a robust modular quantum information processing device. The relatively large dipole moment of the RX qubit compared to double-dot qubits, arising from the more delocalized three-electron wave function within a triple quantum dot device,^{17,18} should enable each RX qubit to interact strongly with the resonator field. At the same time, the smaller size of the triple dot relative to that of, e.g., a transmon^{47,48} should prove useful in scaling to more qubits. Furthermore, the enhanced protection of the RX qubit from low-frequency charge noise at its optimal operating point in principle leads to coherence times sufficiently long for realizing the strong coupling regime.¹⁸

We begin by deriving the form of the coupling between a single RX qubit and a transmission line resonator. Concurrent work investigates this coupling in detail from a microscopic perspective.⁶⁸ Subsequently, we analyze three specific approaches for resonator-mediated entanglement of RX qubits based on techniques drawn from both circuit QED and Hartmann-Hahn double resonance in NMR.⁶⁹ For each of these approaches, we explicitly derive the form of the interaction and construct two-qubit entangling gates. Finally, we explore the feasibility of implementing our proposed gates using RX qubits defined within silicon triple quantum dots. We find that silicon provides qubit relaxation times several orders of magnitude longer than those for GaAs¹⁸ and calculate gate fidelities for the three approaches in the presence of qubit dephasing and cavity decay. Our results suggest that the longer coherence times expected for RX qubits in silicon enable the strong coupling regime to be attained with currently achievable resonator quality factors and should lead to high-fidelity two-qubit entangling gates in combination with rapid, exchange-based universal single-qubit control.^{17,18}

II. DIPOLE COUPLING OF A RESONANT EXCHANGE QUBIT TO A TRANSMISSION LINE RESONATOR

We consider a resonant exchange (RX) qubit, realized within a linear triple quantum dot in the three-electron regime.^{17,18} In the present work, we follow Ref. 18 and focus on the subspace of three-electron states having total spin $S = 1/2$ and spin quantum number for the total z component $m_s = 1/2$ in the charge subspaces $(2,0,1)$, $(1,1,1)$, and $(1,0,2)$ (Fig. 1). Here, (n_1, n_2, n_3) denotes the charge occupation of each dot (numbered from left to right). We assume that a uniform external magnetic field is applied in the plane of the device¹⁶ in order to minimize its effect on the superconducting state of the resonator⁷⁰ and is sufficiently large (typically $\gtrsim 100$ mT¹⁷) such that other three-electron states are energetically distant from the subspace we consider.¹⁸ For RX qubits implemented

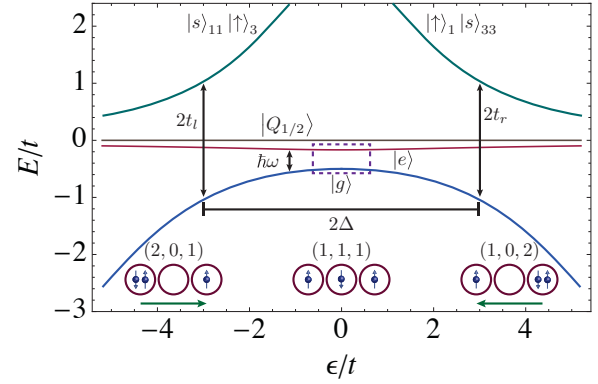


Figure 1. Energy levels of a three-electron triple quantum dot in the $(1,1,1)$, $(2,0,1)$, and $(1,0,2)$ charge subspaces and the $m_s = 1/2$ spin subspace as a function of ϵ/t for $\Delta/t = 3$, with $t = t_l = t_r$. A large uniform external magnetic field (for which the Zeeman splitting is much larger than t) is assumed to separate the subspace considered in the present work from other three-electron states, and the remaining nearby state $|Q_{1/2}\rangle$ has $S = 3/2$.¹⁸ The operating point considered in the present work is indicated by a dotted rectangle. Insets illustrate schematically the electric dipole moments of the triple dot in the $(2,0,1)$ and $(1,0,2)$ configurations.

in silicon, we also assume that excited valley states are well-separated in energy from the lowest-energy valley manifold (see Sec. IV). The resulting subspace is spanned by the $(1,1,1)$ states

$$\begin{aligned} |e_0\rangle &\equiv |s\rangle_{13} |\uparrow\rangle_2 \\ &= \frac{1}{\sqrt{2}} \left(c_{1\uparrow}^\dagger c_{2\uparrow}^\dagger c_{3\downarrow}^\dagger - c_{1\downarrow}^\dagger c_{2\uparrow}^\dagger c_{3\uparrow}^\dagger \right) |\text{vac}\rangle, \\ |g_0\rangle &\equiv \sqrt{\frac{2}{3}} |t_+\rangle_{13} |\downarrow\rangle_2 - \sqrt{\frac{1}{3}} |t_0\rangle_{13} |\uparrow\rangle_2 \\ &= \frac{1}{\sqrt{6}} \left(2c_{1\uparrow}^\dagger c_{2\downarrow}^\dagger c_{3\uparrow}^\dagger - c_{1\uparrow}^\dagger c_{2\uparrow}^\dagger c_{3\downarrow}^\dagger - c_{1\downarrow}^\dagger c_{2\uparrow}^\dagger c_{3\uparrow}^\dagger \right) |\text{vac}\rangle, \end{aligned} \quad (1)$$

along with the $(2,0,1)$ and $(1,0,2)$ states

$$|s_{1,1/2}\rangle \equiv |s\rangle_{11} |\uparrow\rangle_3 = c_{1\uparrow}^\dagger c_{1\downarrow}^\dagger c_{3\uparrow}^\dagger |\text{vac}\rangle, \quad (3)$$

$$|s_{3,1/2}\rangle \equiv |\uparrow\rangle_1 |s\rangle_{33} = c_{1\uparrow}^\dagger c_{3\uparrow}^\dagger c_{3\downarrow}^\dagger |\text{vac}\rangle, \quad (4)$$

where $c_{i\sigma}^\dagger$ is the creation operator for an electron in dot i with spin σ , and $|\text{vac}\rangle$ denotes the vacuum.

When restricted to the $(1,1,1)$ charge subspace, these states also define the originally proposed exchange-only qubit.¹⁴ As discussed in detail in Ref. 18, the RX qubit is defined within an effective $(1,1,1)$ subspace, spanned by the states $|g_0\rangle$ and $|e_0\rangle$ obtained via elimination of the higher-energy three-electron states with charge configurations $(2,0,1)$ and $(1,0,2)$ in Eqs. (3) and (4) using a Schrieffer-Wolff transformation. Defining $\tilde{\sigma}^z \equiv |e_0\rangle\langle e_0| - |g_0\rangle\langle g_0|$, the resulting effective Hamiltonian in

this subspace is given by

$$H_{\text{eff}} = \frac{J}{2} \tilde{\sigma}^z - \frac{\sqrt{3}}{2} j \tilde{\sigma}^x, \quad (5)$$

with $J \equiv (J_l + J_r)/2$, $j \equiv (J_l - J_r)/2$, and where the exchange between the center and left (right) dots is $J_l = t_l^2/(\Delta + \epsilon)$ [$J_r = t_r^2/(\Delta - \epsilon)$]. Here, t_l and t_r are the corresponding tunneling amplitudes, $\epsilon \equiv (V_3 - V_1)/2$ is the detuning parameter for the RX qubit with on-site energies $-V_1$ and $-V_3$ for the left and right dots, respectively, and Δ is defined in terms of Hubbard model parameters such that $\Delta + \epsilon$ ($\Delta - \epsilon$) is the energy of the state $|s_{1,1/2}\rangle$ ($|s_{3,1/2}\rangle$) relative to that of the states $|g_0\rangle$ and $|e_0\rangle$ (see Ref. 18 for more details). In Eq. (5) and the expressions given throughout the remainder of this work, we neglect terms proportional to the identity operator unless otherwise noted. Importantly, while the uniform charge state (1,1,1) of a three-electron triple dot does not interact directly with the microwave field of the resonator, the logical states of the RX qubit contain small admixtures of the polarized charge states (2,0,1) and (1,0,2), enabling coupling to the resonator field (Fig. 1).

In order to determine the strength of this coupling, we first consider the electric dipole transition matrix element for the RX qubit. We take the centers of the three dots to be located at positions $\mathbf{r}_1 = -(w/2)\hat{x}$, $\mathbf{r}_2 = \mathbf{0}$, and $\mathbf{r}_3 = (w/2)\hat{x}$. The dipole operator for the triple dot can then be written as $\mathbf{d} = -e \sum_j \mathbf{r}_j n_j \equiv d\hat{x}$, where $d = \frac{ew}{2}(n_1 - n_3)$ and e is the magnitude of the electron charge. In the chosen subspace $\{|e_0\rangle, |g_0\rangle, |s_{1,1/2}\rangle, |s_{3,1/2}\rangle\}$, the dipole operator takes the form

$$d = \frac{ew}{2} (|s_{1,1/2}\rangle \langle s_{1,1/2}| - |s_{3,1/2}\rangle \langle s_{3,1/2}|). \quad (6)$$

Applying the same Schrieffer-Wolff transformation used to obtain H_{eff} [Eq. (5)] then yields

$$\tilde{d} = \frac{ew}{2} \left(\frac{1}{2} \partial_\epsilon J \tilde{\sigma}^z - \frac{\sqrt{3}}{2} \partial_\epsilon j \tilde{\sigma}^x \right) = \frac{ew}{2} \partial_\epsilon H_{\text{eff}}. \quad (7)$$

Introducing a small variation F in the detuning such that $\epsilon = \epsilon_0 + F$, we write the Hamiltonian of the RX qubit as $H \approx H_{\text{eff}}|_{\epsilon=\epsilon_0} + \partial_\epsilon H_{\text{eff}}|_{\epsilon=\epsilon_0} F$. Note that by comparing this expansion with the expression for \tilde{d} in Eq. (7), the second term of H can be identified with the standard dipole coupling Hamiltonian. The operating point $\epsilon = \epsilon_0$ for the RX qubit is chosen such that the coupling to F , which is proportional to $\partial_\epsilon H_{\text{eff}}$, is perpendicular to the quantization axis in a Bloch sphere representation of the RX qubit. This choice corresponds to the condition $\partial_\epsilon J = -(3j/J) \partial_\epsilon j$. Defining $\sigma^z \equiv |e\rangle \langle e| - |g\rangle \langle g|$, where $\{|g\rangle, |e\rangle\}$ is the basis that diagonalizes H_{eff} [Eq. (5)], the Hamiltonian for small variations of the detuning about the operating point $\epsilon = \epsilon_0$ is given by

$$H_{\text{RX}} = \frac{\hbar\omega}{2} \sigma^z + F\eta \sigma^x, \quad (8)$$

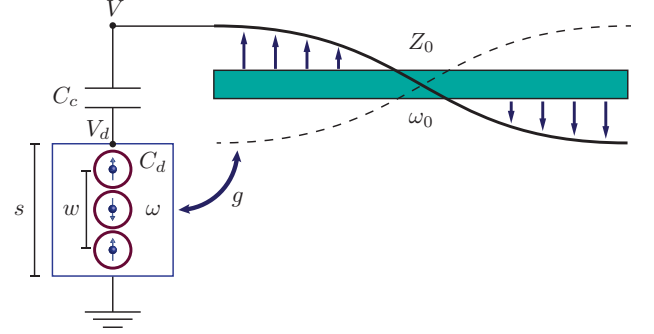


Figure 2. Schematic illustration of the geometry and parameters used to determine the RX qubit-resonator coupling strength g . For clarity, only the center conductor of the resonator is shown.

where $\hbar\omega \equiv \sqrt{J^2 + 3j^2}$ and $\eta \equiv \frac{1}{2} \sqrt{(\partial_\epsilon J)^2 + 3(\partial_\epsilon j)^2} \Big|_{\epsilon=\epsilon_0}$. Thus, the effective dipole transition matrix element for the RX qubit is given by

$$\langle g|d|e\rangle = \frac{ew}{2} \eta = \frac{ew}{4} \sqrt{(\partial_\epsilon J)^2 + 3(\partial_\epsilon j)^2} \Big|_{\epsilon=\epsilon_0}. \quad (9)$$

We now determine the coupling strength for the interaction of the RX qubit with the lowest-energy mode of a transmission line resonator (Fig. 2). A resonator of length l , capacitance per unit length C_0 , and inductance per unit length L_0 has a characteristic impedance $Z_0 = \sqrt{L_0/C_0}$. The fundamental mode of the resonator has frequency $\omega_0 = \pi/lZ_0C_0$ and is described by the quantized antinode voltage^{49,56}

$$\hat{V} = \sqrt{\frac{\hbar\omega_0}{lC_0}} (a + a^\dagger). \quad (10)$$

where a and a^\dagger are resonator photon creation and annihilation operators. We assume a geometry of the type shown in Fig. 2 for the capacitive coupling between the resonator and the triple dot, with the antinodes of the resonator field positioned at the two ends of the center conductor of the resonator. In terms of the total capacitance C_c between the resonator and the triple dot and the total capacitance C_d between the triple dot and ground, the voltage across the triple dot is given by $\hat{V}_d = C_c \hat{V} / (C_c + C_d) \equiv v \hat{V}$. The interaction of the RX qubit with this voltage, described by $H_{\text{int}} = -\mathbf{d} \cdot \mathbf{E} = d\hat{V}_d/s$, where s is the effective distance over which the voltage drop \hat{V}_d occurs, then takes the form

$$H_{\text{int}} = \hbar g_0 (n_1 - n_3) (a + a^\dagger), \quad (11)$$

with the vacuum Rabi coupling

$$g_0 \equiv \frac{ewv}{2slC_0} \sqrt{\frac{\pi}{Z_0\hbar}} = \frac{ewv}{2s} \omega_0 \sqrt{\frac{Z_0}{\pi\hbar}}. \quad (12)$$

In the representation $\{|\tilde{e}_0\rangle, |\tilde{g}_0\rangle\}$, the operator $(n_1 - n_3)$ becomes $\partial_\epsilon H_{\text{eff}}$. Since the dipole coupling Hamiltonian $\tilde{H}_{\text{int}} = \partial_\epsilon H_{\text{eff}}|_{\epsilon=\epsilon_0} F$ as discussed above, we also note that the interaction with the transmission line resonator is described by quantizing F and setting $F = ew\hat{V}_d/2s$ so that the oscillation in the detuning of the RX qubit is controlled by the resonator voltage. At the operating point $\epsilon = \epsilon_0$, which corresponds to $\partial_\epsilon J = -(3j/J)\partial_\epsilon j$, the interaction Hamiltonian in the qubit basis $\{|g\rangle, |e\rangle\}$ takes the form

$$H'_{\text{int}} = \hbar g \sigma^x (a + a^\dagger), \quad (13)$$

where the effective qubit-resonator coupling strength is given by

$$g \equiv \eta g_0 = \frac{g_0}{2} \sqrt{(\partial_\epsilon J)^2 + 3(\partial_\epsilon j)^2} \Big|_{\epsilon=\epsilon_0}. \quad (14)$$

To estimate the interaction strength g , we choose $\epsilon_0 = 0$ as the operating point for the qubit (see Fig. 1). At this point, $J_l = J_r = t^2/\Delta$, while $\partial_\epsilon J = 0$ and $\partial_\epsilon j = -t^2/\Delta^2$. Defining the charge admixture parameter $\xi \equiv t/\Delta$, this gives $\eta = \sqrt{3}\xi^2/2$. For simplicity, we set $s = w$ in Eq. (12). Choosing $Z_0 = 50 \Omega$, $v = 0.28$,^{42,49} and $\omega_0 = 2\pi \times 1.5 \text{ GHz}$ ⁵⁶ (where we assume $k_B T \ll \hbar\omega_0$ in order to neglect thermal excitation of photons) leads to a charge-cavity coupling strength $g_0 \approx 2\pi \times 13 \text{ MHz}$. Taking $\xi = 0.3$,¹⁸ we then find $g \approx 2\pi \times 1 \text{ MHz}$ for the strength of the coupling between the RX qubit and the transmission line resonator, which is comparable to that found experimentally for spin qubits in double quantum dots coupled to a higher-frequency resonator.⁵⁹ We note that, while the qubit-resonator coupling strength g is limited by the constraint $\xi \ll 1$ required for the validity of the Heisenberg model description of the RX qubit,¹⁸ the estimate we obtain here does not represent a fundamental limit and varies strongly with the chosen parameters. Further enhancements of g may be possible by, e.g., modifying the design of the transmission line resonator to increase the strength of the electric field within the region containing the RX qubit^{60,70} and thus the charge-cavity coupling strength g_0 . Recent work⁷⁰ demonstrates a characteristic impedance $Z_0 \approx 4 \text{ k}\Omega$ for superconducting nanowire resonators with high kinetic inductance, which leads to $g_0 \approx 2\pi \times 120 \text{ MHz}$ and $g \approx 2\pi \times 9 \text{ MHz}$ for the same values of ω_0 , v and ξ chosen above.

The value of g we determine here is nevertheless sufficient for reaching the strong coupling regime of the RX qubit-resonator interaction in realistic systems, as we now show. The strong coupling regime corresponds to $g > \kappa, \gamma$, where $\kappa = \omega_0/Q$ is the rate of decay of microwave photons out of the resonator, Q is the resonator quality factor, and $\gamma = 1/T_2^*$ is the qubit decay rate.^{42,49} This regime is characterized by a transfer of excitations between the qubit and the resonator that is more rapid than the qubit and photon decay rates and is thus of fundamental importance for resonator-mediated

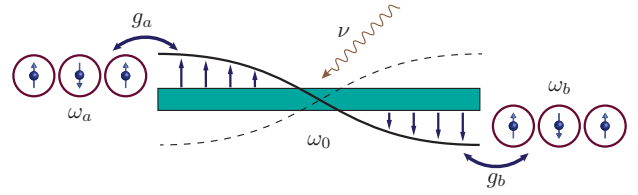


Figure 3. Schematic showing two resonant exchange (RX) qubits, having transition frequencies ω_a and ω_b , coupled to the fundamental mode of a microwave transmission line resonator, having frequency ω_0 , with strengths g_a and g_b , respectively. An external microwave driving field of frequency ν applied to the resonator is also indicated.

entangling gates. For the estimated coupling strength $g = 2\pi \times 9 \text{ MHz}$ and $\omega_0 = 2\pi \times 1.5 \text{ GHz}$, the strong coupling regime can be achieved when the conditions $Q > \omega_0/g \approx 160$ and $T_2^* > 1/g \approx 17 \text{ ns}$ are satisfied. Recent experiments^{50,53,59} suggest that sufficiently high quality factors are already attainable in coupled dot-resonator systems. In addition, a single RX qubit implemented in a GaAs triple quantum dot has a dephasing time $T_2^* \approx 500 \text{ ns}$, and an increase of the coherence time to $T_2 \approx 20 \mu\text{s}$ via echo has been demonstrated.¹⁷ The strong coupling regime should therefore be attainable for $\xi \ll 0.3$, which is advantageous for RX qubits in GaAs dots as the rate of qubit decay due to phonons is expected to increase as $\sim \xi^4$.¹⁸ In Sec. IV, we consider relaxation due to electron-phonon coupling for RX qubits in Si triple dots and find that, for this system, phonon-induced decay is unlikely to limit qubit coherence. Thus, Si-based RX qubits should in principle enable operation in the strong coupling regime for larger dipole moments (i.e., larger $\eta \sim \xi^2$), which should lead to more rapid entangling gates.

III. RESONATOR-MEDIATED ENTANGLING GATES FOR TWO RX QUBITS

We now explore three specific approaches for entangling two spatially separated RX qubits which are both coupled to the fundamental mode of a transmission line resonator via their electric dipole moments (Fig. 3). As we show below, methods developed for coupling superconducting qubits in circuit QED^{42,44} along with Hartmann-Hahn double resonance techniques for externally driven systems⁶⁹ can be directly applied to RX qubits, in combination with fast single-qubit rotations via exchange. We explicitly derive the effective interactions and the two-qubit entangling gates they generate for each approach, while including relevant prior results from circuit QED for completeness.

In Sec. III A, we consider the interaction between two RX qubits with identical transition frequencies mediated by virtual excitations of the resonator in the dispersive regime, which gives rise to gate rates $\sim g^2/\tilde{\Delta} \sim \xi^4$, where $\tilde{\Delta}$ denotes the detuning of the qubit transition frequency

with respect to the resonator frequency. We describe an alternative approach in Sec. III B, which involves driving each qubit with resonant microwave fields to generate sideband transitions in a doubly rotating frame. This approach leads to a gate rate that scales linearly with the coupling strength $g \sim \xi^2$, potentially providing a faster gate than that discussed in Sec. III A. Finally, we consider the dispersive regime for the driven resonator-mediated interaction between two RX qubits having different transition frequencies in Sec. III C. We show how transforming to a doubly rotating frame enables two-qubit entangling gates with rates $\sim \xi^4$ even in the presence of the qubit frequency variation.

Identifying the regime which optimizes two-qubit gate fidelities for a particular implementation involves a comparison of the qubit and resonator photon coherence times. Two-qubit gates in the dispersive regime are expected to have higher fidelities for systems where the qubit coherence time exceeds the resonator photon coherence time, as the interaction is mediated only by virtual resonator photons. On the other hand, fidelities for two-qubit gates based on the direct qubit-resonator interaction in the resonant regime are limited by both the qubit and the resonator photon coherence times. In Sec. V, we show that this intuition is consistent with calculated gate fidelities for the three regimes we consider.

A. Dispersive regime

Initially, we consider two RX qubits coupled to the resonator in the absence of external driving fields. Using Eqs. (8) and (13), the Hamiltonian of the combined system can be written as $H_d = H_0 + V$, where (setting $\hbar = 1$)

$$H_0 = \omega_0 a^\dagger a + \sum_{\mu=a,b} \frac{\omega_\mu}{2} \sigma_\mu^z \quad (15)$$

describes the individual RX qubits (having transition frequencies ω_a and ω_b) together with the fundamental mode of the resonator (having frequency ω_0), and

$$V = \sum_{\mu=a,b} g_\mu \sigma_\mu^x (a + a^\dagger) \quad (16)$$

describes the dipolar interaction of the RX qubits with the resonator. Thus, H_d is of the Jaynes-Cummings form⁷¹ with $g_\mu \equiv \eta_\mu g_0^\mu$ representing the strength of the coupling to the resonator for qubit $\mu = a, b$. By using $\sigma_\mu^x = \sigma_\mu^+ + \sigma_\mu^-$, where $\sigma_\mu^+ \equiv |e\rangle\langle g|$ and $\sigma_\mu^- \equiv |g\rangle\langle e|$, defining the qubit-resonator detunings $\tilde{\Delta}_\mu \equiv \omega_0 - \omega_\mu$, and applying a rotating wave approximation for $|\tilde{\Delta}_\mu| \ll \omega_0 + \omega_\mu$ in order to neglect the energy-nonconserving terms containing $\sigma_\mu^+ a^\dagger$ and $\sigma_\mu^- a$, Eq. (16) can be approximated as

$$V \approx \sum_{\mu=a,b} g_\mu (\sigma_\mu^+ a + \sigma_\mu^- a^\dagger). \quad (17)$$

The effective two-qubit interaction mediated by the resonator between the RX qubits in the dispersive regime, defined by $g_\mu \ll |\tilde{\Delta}_\mu|$ for $\mu = a, b$, is obtained via a Schrieffer-Wolff transformation that eliminates the direct qubit-resonator coupling [Eq. (17)] to first order in $g_\mu/\tilde{\Delta}_\mu$.^{42,44,55} The resulting effective Hamiltonian can be approximated as $\tilde{H}_d \equiv H_0 + \frac{1}{2} [S_1, V]$, where

$$S_1 \equiv - \sum_{\mu=a,b} \frac{g_\mu}{\tilde{\Delta}_\mu} (\sigma_\mu^+ a - \sigma_\mu^- a^\dagger). \quad (18)$$

We express the result in the form $\tilde{H}_d = \tilde{H}_0 + \tilde{V}$, with

$$\tilde{H}_0 \equiv H_0 - \sum_{\mu=a,b} \frac{g_\mu^2}{\tilde{\Delta}_\mu} \left(a^\dagger a + \frac{1}{2} \right) \sigma_\mu^z, \quad (19)$$

$$\tilde{V} \equiv -\chi_{ab} (\sigma_a^+ \sigma_b^- + \sigma_a^- \sigma_b^+), \quad (20)$$

where we define the two-qubit coupling strength

$$\chi_{ab} \equiv \frac{g_a g_b}{2} \left(\frac{1}{\tilde{\Delta}_a} + \frac{1}{\tilde{\Delta}_b} \right). \quad (21)$$

To obtain the two-qubit entangling gate generated by \tilde{H}_d , we focus on the zero-photon two-qubit subspace $\{|e, e, 0\rangle, |e, g, 0\rangle, |g, e, 0\rangle, |g, g, 0\rangle\}$. Here, $|n\rangle$ denotes the n -photon state of the resonator, with $n = 0, 1, 2, \dots$. In this subspace, we find

$$\begin{aligned} \tilde{H}_d^{(0)} &\equiv \langle 0 | \tilde{H}_d | 0 \rangle \\ &= \sum_{\mu=a,b} \frac{\omega'_\mu}{2} \sigma_\mu^z \\ &\quad - \chi_{ab} (\sigma_a^+ \sigma_b^- + \sigma_a^- \sigma_b^+). \end{aligned} \quad (22)$$

Eq. (22) is expressed in terms of the modified qubit transition frequency

$$\omega'_\mu \equiv \omega_\mu - \frac{g_\mu^2}{\tilde{\Delta}_\mu}. \quad (23)$$

We now transform $\tilde{H}_d^{(0)}$ to a rotating frame via

$$U_{\text{rf}} = e^{-i(\omega'_a \sigma_a^z + \omega'_b \sigma_b^z)\tau/2}. \quad (24)$$

This leads to

$$\begin{aligned} H_d^{\text{rf}} &= U_{\text{rf}}^\dagger \tilde{H}_d^{(0)} U_{\text{rf}} - i U_{\text{rf}}^\dagger \dot{U}_{\text{rf}} \\ &= -\chi_{ab} \left[\sigma_a^+ \sigma_b^- e^{i(\omega'_a - \omega'_b)\tau} + \sigma_a^- \sigma_b^+ e^{-i(\omega'_a - \omega'_b)\tau} \right] \end{aligned} \quad (25)$$

Note that both U_d and H_d^{rf} act only within the zero-photon subspace. When the transition frequencies of the two qubits are resonant with each other, so that $\omega'_a = \omega'_b$, we find

$$H_d^{\text{rf}} \approx -\frac{g_a g_b}{\tilde{\Delta}} (\sigma_a^+ \sigma_b^- + \sigma_a^- \sigma_b^+), \quad (26)$$

where we have dropped small terms $\sim g_\mu^2/\tilde{\Delta}_\mu^2$ so that $\tilde{\Delta}_a^{-1} \approx \tilde{\Delta}_b^{-1} \equiv \tilde{\Delta}^{-1}$.

The unitary evolution generated by the interaction in Eq. (26) is described by the operator⁴²

$$U_d(\tau) \equiv e^{-iH_d^{\text{rf}}\tau} = \begin{pmatrix} 1 & & & \\ & \cos\left(\frac{g_a g_b \tau}{\tilde{\Delta}}\right) & i \sin\left(\frac{g_a g_b \tau}{\tilde{\Delta}}\right) & \\ & i \sin\left(\frac{g_a g_b \tau}{\tilde{\Delta}}\right) & \cos\left(\frac{g_a g_b \tau}{\tilde{\Delta}}\right) & \\ & & & 1 \end{pmatrix}. \quad (27)$$

For $\tau = \tau_n \equiv (4n+1)\pi\tilde{\Delta}/2g_a g_b$, where n is an integer, Eq. (27) yields the i SWAP gate. This two-qubit entangling gate can be combined with single qubit rotations to form a universal set of quantum gates.⁷² The gate U_d has a rate given by $g_a g_b/\tilde{\Delta} \sim g^2/\tilde{\Delta} \sim \xi^4$, where we assume $g_b \sim g_a \equiv g$.

B. Driven resonant regime

The two-qubit entangling gates considered in Sec. III A have rates that scale as $g^2/\tilde{\Delta} \sim \xi^4$. Thus, these gates are limited in speed by both the condition $\xi \ll 1$ for the validity of the Heisenberg model¹⁸ and the fact that they are carried out in the dispersive regime, where $g \ll \tilde{\Delta}$. In order to obtain more rapid gates with rates that vary linearly with $g \sim \xi^2$, we now consider an alternative approach for generating entanglement between two RX qubits based on microwave driving of sideband transitions,^{44,73,74} in the spirit of the Cirac-Zoller gate for two-level ions.^{75,76} When a microwave driving field resonant with one of the qubit transitions is applied to the resonator, the qubit-resonator interaction [Eq. (13)] enables driving of the qubit at its Rabi frequency. In a frame rotating at both the drive and Rabi frequencies, the interaction of the resonator with each qubit leads to sideband transitions for appropriately chosen frequencies of the driving field.⁴⁴ These transitions can be used to construct two-qubit entangling gates.^{75,76} Here, we show how this approach applies directly to two RX qubits coupled to a transmission line resonator and explicitly derive the full gate sequence for a controlled-Z (π -phase) gate.

To obtain the effective Hamiltonians which generate sideband transitions, we begin by considering the interaction of a single RX qubit with the resonator in the presence of an external driving field. Writing Eqs. (15) and (16) for a single qubit and adding a term describing driving of the resonator (see Fig. 3) by an applied microwave field of frequency ν , amplitude ε , and phase ϕ gives

$$H_r = \omega_0 \tilde{a}^\dagger \tilde{a} + \frac{\omega}{2} \sigma^z + g \sigma^x (\tilde{a} + \tilde{a}^\dagger) + \varepsilon \left[e^{-i(\nu\tau+\phi)} \tilde{a}^\dagger + e^{i(\nu\tau+\phi)} \tilde{a} \right], \quad (28)$$

where we use a modified notation for the resonator mode operators \tilde{a} and \tilde{a}^\dagger for convenience in later expressions. We work in a regime where the driving field amplitude ε and the detuning $\Delta_0 \equiv \omega_0 - \nu$ are sufficiently large that we can neglect the quantum fluctuations of the driving field arising from its interaction with the resonator and approximate the drive as a classical field.⁴⁴ In this regime, we can eliminate terms describing the direct action of the drive on the resonator from the Hamiltonian by applying a displacement transformation using $D(\alpha) \equiv e^{\alpha \tilde{a}^\dagger - \alpha^* \tilde{a}}$ and setting $\alpha(\tau)$ equal to the steady-state solution of $\dot{\alpha} + i\omega_0 \alpha + i\varepsilon e^{-i(\nu\tau+\phi)} = 0$, which gives $\alpha(\tau) = -\varepsilon e^{-i(\nu\tau+\phi)}/\Delta_0$. This choice of α yields

$$\begin{aligned} H'_r &= D^\dagger(\alpha) H_r D(\alpha) - iD^\dagger(\alpha) \dot{D}(\alpha) \\ &= \omega_0 \tilde{a}^\dagger \tilde{a} + \frac{\omega}{2} \sigma^z + g \sigma^x (\tilde{a} + \tilde{a}^\dagger) \\ &\quad - 2\Omega \cos(\nu\tau + \phi) \sigma^x, \end{aligned} \quad (29)$$

where

$$2\Omega \equiv \frac{2g\varepsilon}{\Delta_0} \quad (30)$$

is the Rabi frequency for the qubit.

We next transform to a frame rotating at the drive frequency ν using the unitary transformation

$$U_1 = e^{-i\nu\tau(\tilde{a}^\dagger \tilde{a} + \sigma^z/2)}. \quad (31)$$

Driving the qubit on resonance, so that $\nu = \omega$, and dropping rapidly oscillating terms $\sim e^{\pm 2i\nu\tau}$ leads to

$$\begin{aligned} H_r^{\text{rf}} &= \Delta_0 \tilde{a}^\dagger \tilde{a} + g (\sigma^+ \tilde{a} + \sigma^- \tilde{a}^\dagger) \\ &\quad - \Omega (e^{-i\phi} \sigma^+ + e^{i\phi} \sigma^-). \end{aligned} \quad (32)$$

For convenience, we rotate H_r^{rf} such that the last term becomes proportional to σ^y . This can be achieved using the transformation

$$U_{\text{rot}} = e^{-i(\phi+\pi/2)\sigma^z/2}. \quad (33)$$

Letting $a \equiv i\tilde{a}$, we can express the rotated Hamiltonian as

$$\begin{aligned} H_r^{\text{rot}} &= U_{\text{rot}}^\dagger H_r^{\text{rf}} U_{\text{rot}} \\ &= \Delta_0 a^\dagger a + g (e^{i\phi} \sigma^+ a + e^{-i\phi} \sigma^- a^\dagger) + \Omega \sigma^y. \end{aligned} \quad (34)$$

Eq. (34) gives the Hamiltonian for one RX qubit coupled to a resonator and driven by an external microwave field, in a frame rotating at its resonance frequency $\nu = \omega$. In order to obtain interaction terms that generate sideband transitions, we now transform H_r^{rot} to a second frame rotating at the Rabi frequency 2Ω for the qubit and at the effective frequency Δ_0 for the resonator using

$$U_2 = e^{-i(\Delta_0 a^\dagger a + \Omega \sigma^y)\tau}. \quad (35)$$

This unitary transformation yields

$$H_r^{\text{drf}} = \frac{g}{2} [\cos(2\Omega\tau) \sigma^x + \sin(2\Omega\tau) \sigma^z] \times (e^{i\phi} e^{-i\Delta_0\tau} a + e^{-i\phi} e^{i\Delta_0\tau} a^\dagger) + i \frac{g}{2} \sigma^y (e^{i\phi} e^{-i\Delta_0\tau} a - e^{-i\phi} e^{i\Delta_0\tau} a^\dagger), \quad (36)$$

which describes the interaction of the RX qubit with the resonator in terms of a time-dependent rotation of the transition dipole moment induced by the Rabi frequency. Finally, applying the transformation

$$U'_{\text{rot}} = e^{i(\pi/4)\sigma^x}, \quad (37)$$

to H_r^{drf} yields

$$\tilde{H}_r^{\text{drf}} = \frac{g}{2} \left[e^{i\phi} e^{-i(\Delta_0-2\Omega)\tau} \sigma^+ a + e^{-i\phi} e^{i(\Delta_0-2\Omega)\tau} \sigma^- a^\dagger + e^{-i\phi} e^{i(\Delta_0+2\Omega)\tau} \sigma^+ a^\dagger + e^{i\phi} e^{-i(\Delta_0+2\Omega)\tau} \sigma^- a \right] + i \frac{g}{2} \sigma^z (e^{i\phi} e^{-i\Delta_0\tau} a - e^{-i\phi} e^{i\Delta_0\tau} a^\dagger). \quad (38)$$

Based on the form of Eq. (38), we make a rotating wave approximation for two cases. First, we set $\Delta_0 = 2\Omega$ in Eq. (38) and neglect the rapidly oscillating terms containing $\sigma^+ a^\dagger$, $\sigma^- a$, $\sigma^z a$, and $\sigma^z a^\dagger$ to obtain

$$H_- = \frac{g}{2} (e^{i\phi} \sigma^+ a + e^{-i\phi} \sigma^- a^\dagger). \quad (39)$$

Alternatively, setting $\Delta_0 = -2\Omega$, we find that the rapidly oscillating terms are those containing $\sigma^+ a$, $\sigma^- a^\dagger$, $\sigma^z a$, and $\sigma^z a^\dagger$. After dropping these terms, Eq. (38) becomes

$$H_+ = \frac{g}{2} (e^{-i\phi} \sigma^+ a^\dagger + e^{i\phi} \sigma^- a). \quad (40)$$

The Hamiltonians H_- and H_+ generate “red” and “blue” sideband transitions, respectively,^{44,76} as can be verified by considering their action on the qubit-resonator basis states $|g, n\rangle$ and $|e, n\rangle$ (Fig. 4). The gates generated by H_\pm can be expressed as^{44,76}

$$S^-(\theta, \phi) = e^{-i(\theta/2)(e^{i\phi} \sigma^+ a + e^{-i\phi} \sigma^- a^\dagger)}, \quad (41)$$

$$S^+(\theta, \phi) = e^{-i(\theta/2)(e^{-i\phi} \sigma^+ a^\dagger + e^{i\phi} \sigma^- a)}, \quad (42)$$

where $\theta \equiv g\tau$. Thus, although $\omega \neq \omega_0$, driving each RX qubit resonantly and moving to a doubly rotating frame via U_1 and U_2 [Eqs. (31) and (35)] generates sideband transitions that transfer excitations between the qubit and the resonator via an effective resonance in the doubly rotating frame that is enabled by the combination of the drive and resonator photons.

We now construct a controlled-phase gate for two RX qubits using Eqs. (41) and (42). Here, we focus on the controlled-Z (π -phase) gate. Following the approach of Ref. 76, we use a sequence of red sideband transitions to define the gate

$$W \equiv S^-\left(\frac{\pi}{2}, 0\right) S^-\left(\pi\sqrt{2}, \frac{\pi}{2}\right) S^-\left(-\frac{\pi}{2}, 0\right), \quad (43)$$

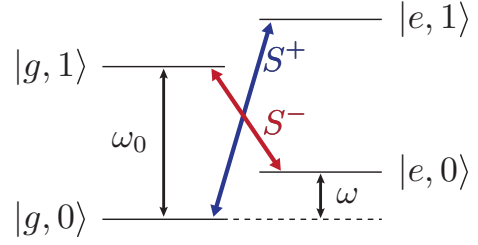


Figure 4. Red (S^-) and blue (S^+) sideband transitions [Eqs. (41) and (42), respectively] generated in the doubly rotating frame for a single RX qubit coupled to a resonator and driven on resonance ($\nu = \omega$).

which acts on a single qubit coupled to the resonator. As discussed in Ref. 76, this gate plays a role equivalent to the 2π pulse used in the Cirac-Zoller sequence for trapped ions⁷⁵ but requires only the two levels of a qubit, in contrast to resonant approaches proposed for superconducting qubits.⁷⁷ As W also prevents leakage to resonator states other than $|0\rangle$ and $|1\rangle$, we can consider the subspace $\{|g, 0\rangle, |g, 1\rangle, |e, 0\rangle, |e, 1\rangle\}$. In this basis, Eq. (43) has the form

$$W = \begin{pmatrix} 1 & & & \\ & e^{-i\pi/\sqrt{2}} & & \\ & & e^{i\pi/\sqrt{2}} & \\ & & & -1 \end{pmatrix}. \quad (44)$$

Combining the gate W with additional blue sideband transitions and single-qubit z -axis rotations yields the gate sequence

$$U_{\text{CZ}} = R_{z,a}\left(\frac{\pi}{\sqrt{2}}\right) S_a^+(\pi, \phi) W_b R_{z,b}\left(\frac{\pi}{\sqrt{2}}\right) S_a^+(\pi, \phi), \quad (45)$$

where the added subscripts a, b indicate the qubit on which each gate acts. In the zero-photon subspace $\{|e, e, 0\rangle, |e, g, 0\rangle, |g, e, 0\rangle, |g, g, 0\rangle\}$, U_{CZ} takes the form of a controlled-Z gate with respect to the two-qubit basis states and thus entangles the two qubits.

Note that, in addition to W and additional sideband transitions, the full sequence for the controlled-Z gate in Eq. (45) requires single-qubit rotations about the z axis of the Bloch sphere for each RX qubit. As seen from Eq. (8), rapid single-qubit rotations for the RX qubit can be generated via exchange.^{17,18} In the absence of detuning variations about the operating point (i.e., for $F = 0$), H_{RX} generates a rotation $R_z(\varphi) \equiv e^{-i(\varphi/2)\sigma^z}$ about the z axis of the Bloch sphere of a RX qubit, with $\varphi = \omega\tau$. With qubit-resonator coupling present, a z -axis rotation for a particular qubit can be carried out by tuning ω such that $|\tilde{\Delta}| \equiv |\omega_0 - \omega| \gg g$, so that $g/|\tilde{\Delta}| \rightarrow 0$ and the interaction of the qubit with the resonator effectively vanishes.

While the qubit frequency must be well-separated from the resonator frequency ω_0 , we note that $\omega \gg g$ is

also satisfied for typical system parameters (e.g., $\omega \sim 2\pi \times 1$ GHz¹⁸ and $g \lesssim 2\pi \times 10$ MHz). Thus, we expect the two-qubit gate rate to be limited by that of the sideband gates. As all sideband gates in Eq. (45) are generated by interactions that depend linearly on the coupling strength g via $\theta = g\tau$, and as the exchange-generated single-qubit rotations have a rate $\omega \gg g$, this suggests that the overall two-qubit gate rate scales as $g \sim \xi^2$. The driven resonant regime should therefore enable more rapid gates than those discussed in Sec. III A. We note that the resonant regime of quantum dot-cavity coupling has been achieved in recent experiments,⁷⁸ which demonstrate measurements of the transition to this regime via the observation of an enhanced intensity of the resonant sideband of the Mollow triplet characteristic of a strongly driven two-level system.⁷⁹

C. Driven dispersive regime

Generating entanglement between RX qubits in the presence of variation in their transition frequencies enables both two-qubit gates and addressability of individual qubits. Thus, we now consider the dispersive regime for two qubits coupled to the resonator with $\omega_a \neq \omega_b$. In contrast to the approach of Sec. III A, we also include a microwave driving field acting on the resonator (see Sec. III B and Fig. 3) with a frequency ν equal to the transition frequency of one qubit. Interaction with the resonator shifts both the Rabi frequency of the qubit resonant with the driving field and the difference of the qubit transition frequencies. We derive an entangling gate that is generated by the effective interaction in a frame rotating at both the drive frequency and the modified qubit Rabi and difference frequencies. This doubly rotating frame enables energy exchange between the qubits even when they have different transition frequencies, in analogy to Hartmann-Hahn double resonance in NMR.^{69,80}

From Eqs. (15) and (16), the Hamiltonian is given by

$$H_{dd} = \omega_0 a^\dagger a + \sum_{\mu=a,b} \frac{\omega_\mu}{2} \sigma_\mu^z + \sum_{\mu=a,b} g_\mu \sigma_\mu^x (a + a^\dagger) + \varepsilon \left[e^{-i(\nu\tau+\phi)} a^\dagger + e^{i(\nu\tau+\phi)} a \right], \quad (46)$$

We displace the resonator field using $D(\alpha)$ as in Eq. (29) in order to eliminate the direct action of the driving field on the resonator, obtaining

$$H'_{dd} = \omega_0 a^\dagger a + \sum_{\mu=a,b} \frac{\omega_\mu}{2} \sigma_\mu^z + \sum_{\mu=a,b} g_\mu \sigma_\mu^x (a + a^\dagger) - \sum_{\mu=a,b} 2\Omega_\mu \cos(\nu t + \phi) \sigma_\mu^x, \quad (47)$$

where $2\Omega_\mu \equiv 2g_\mu \varepsilon / \Delta_0$.

We next transform to a rotating frame via

$$U'_1 = e^{-i\nu(a^\dagger a + \sigma_a^z/2 + \sigma_b^z/2)\tau}. \quad (48)$$

Subsequently assuming the driving field is resonant with the transition of qubit a such that $\nu = \omega_a$, setting $\Omega_b = \phi = 0$ for simplicity, and dropping rapidly oscillating terms $\sim e^{\pm 2i\nu\tau}$ leads to

$$H_{dd}^{\text{rf}} \approx \Delta_0 a^\dagger a - \Omega_a \sigma_a^x + \frac{\delta}{2} \sigma_b^z + \sum_{\mu=a,b} g_\mu (\sigma_\mu^+ a + \sigma_\mu^- a^\dagger), \quad (49)$$

where we have defined the qubit frequency difference $\delta \equiv \omega_b - \omega_a = \omega_b - \nu$. We also apply a rotation to qubit a using

$$U_a = e^{i(\pi/4)\sigma_a^y} \quad (50)$$

in order to diagonalize the term with σ_a^x in the second line of Eq. (49). This transformation yields a Hamiltonian $H_{dd}^{\text{rot}} = U_a^\dagger H_{dd}^{\text{rf}} U_a$ which contains additional terms not present in the Hamiltonian H_d considered in Sec. III A for two qubits of equal transition frequencies in the dispersive regime and in the absence of a driving field. In order to simplify the analysis leading to an effective interaction between the two RX qubits in the present case, we apply perturbation theory and take into account only states within the low-energy subspace $\{|0\rangle, |1\rangle\}$ for the resonator. We write $H_{dd}^{\text{rot}} = H'_0 + V_{dd}$, where

$$H'_0 = \Delta_0 a^\dagger a + \Omega_a \sigma_a^z + \frac{\delta}{2} \sigma_b^z, \quad (51)$$

$$V_{dd} = -\frac{g_a}{2} \sigma_a^z (a + a^\dagger) + \frac{g_a}{2} (\sigma_a^+ - \sigma_a^-) (a - a^\dagger) + g_b (\sigma_b^+ a + \sigma_b^- a^\dagger). \quad (52)$$

Assuming $g_{a,b} \ll \Omega_a \approx |\delta| \ll |\Delta_0|$, we consider separately the three subspaces defined by the projection operators $P_+ \equiv |e, e, 0\rangle \langle e, e, 0|$, $P_0 \equiv |e, g, 0\rangle \langle e, g, 0| + |g, e, 0\rangle \langle g, e, 0|$, and $P_- \equiv |g, g, 0\rangle \langle g, g, 0|$. Denoting the the projector for the one-photon subspace by Q , the resulting effective Hamiltonian in the full zero-photon subspace $P \equiv P_+ + P_0 + P_-$ is found to be

$$H_{\text{eff}}^{(0)} \equiv P H_{\text{eff}} P = P H'_0 P + P V_{dd} Q \frac{1}{\varepsilon_0 - Q H'_0 Q} Q V_{dd} P = \tilde{\Omega}_a \sigma_a^z + \frac{\tilde{\delta}}{2} \sigma_b^z - \frac{g_a g_b}{2(\Delta_0 - \delta)} (\sigma_a^+ \sigma_b^- + \sigma_a^- \sigma_b^+), \quad (53)$$

where we have set $2\Omega_a = \delta$ for simplicity, chosen $\varepsilon_0 = 0, \pm\delta$ for $P_{0,\pm}$, respectively, and defined the quantities

$$2\tilde{\Omega}_a \equiv \delta - \frac{g_a^2}{4} \left(\frac{1}{\Delta_0 - \delta} - \frac{1}{\Delta_0 + \delta} \right), \quad (54)$$

$$\tilde{\delta} \equiv \delta - \frac{g_b^2}{\Delta_0 - \delta}. \quad (55)$$

Here, $2\tilde{\Omega}_a$ represents the effective Rabi frequency of RX qubit a and $\tilde{\delta}$ is the effective qubit transition frequency difference when both RX qubits are coupled to the resonator in the dispersive regime.

Finally, we transform to a second rotating frame using the operator

$$U'_2 = e^{-i(\tilde{\Omega}_a \sigma_a^z + \tilde{\delta} \sigma_b^z/2)\tau}, \quad (56)$$

which acts within the zero-photon subspace. This leads to

$$\begin{aligned} \tilde{H}_{\text{eff}}^{(0)} &= -\frac{g_a g_b}{2(\Delta_0 - \delta)} \\ &\times \left[\sigma_a^+ \sigma_b^- e^{i(2\tilde{\Omega}_a - \tilde{\delta})\tau} + \sigma_a^- \sigma_b^+ e^{-i(2\tilde{\Omega}_a - \tilde{\delta})\tau} \right] \end{aligned} \quad (57)$$

We now set $2\tilde{\Omega}_a = \tilde{\delta}$, which from Eqs. (54) and (55) also leads to the constraint

$$g_b = g_a \sqrt{\frac{\delta}{2(\Delta_0 + \delta)}} \quad (58)$$

relating the qubit-resonator coupling strengths. For the effective Hamiltonian in the doubly rotating frame, we then find

$$H_{dd}^{\text{drf}} \approx -\frac{g_a g_b}{2(\Delta_0 - \delta)} (\sigma_a^+ \sigma_b^- + \sigma_a^- \sigma_b^+), \quad (59)$$

where g_b and g_a are related by Eq. (58) for the case $2\Omega_a = \delta$. Thus, driving qubit a such that its Rabi frequency is resonant with the difference between the qubit transition frequencies leads to an effective two-qubit interaction in the doubly rotating frame. Note that this interaction has the same form as (26). The unitary evolution generated by H_{dd}^{drf} is therefore of the same form as Eq. (26) and gives rise to the same two-qubit entangling gates, with a rate $g_a g_b / 2(\Delta_0 - \delta) \sim \sqrt{\delta/\Delta_0} (g^2/\Delta_0) \sim \xi^4$, while additionally allowing for variation in the transition frequencies of the two qubits.

IV. IMPLEMENTATION IN SI TRIPLE QUANTUM DOTS

We now consider the feasibility of implementing the approaches for entangling RX qubits discussed in the present work within silicon quantum dots. Recent work has demonstrated rapid, coherent control of a single RX qubit in a GaAs triple dot.¹⁷ However, in addition to gate voltage noise, the coherence is expected to be further limited in GaAs by the nuclear spin environment

and by piezoelectric phonons,¹⁸ which typically represent the dominant sources of charge and spin relaxation in GaAs quantum dots.⁶ Implementing RX qubits in Si potentially provides improved coherence due to a low nuclear spin concentration, which can be made to approach zero via isotopic purification, as well as to the absence of piezoelectric phonons.^{23,62–67} However, the valley degree of freedom in Si leads to a more complex low-energy spectrum than that of GaAs. Thus, a direct extension of RX qubit properties to Si is not obviously straightforward.

Here, we focus on the effects of relaxation due to electron-phonon coupling in the context of the approaches described in the present work. We assume that each RX qubit is coupled independently to the same phonon bath and calculate the relaxation rate for a single three-electron triple quantum dot in Si. In order to identify the most relevant relaxation transition, we note that a typical single-dot valley splitting $E_V \gtrsim 100 \mu\text{eV}$,^{62,81} while typical qubit frequencies that set the gap between the qubit basis states $|g\rangle$ and $|e\rangle$ correspond to $\hbar\omega < 10 \mu\text{eV}$. Thus, we assume that ω determines the lowest relevant gap for the RX qubit and that the dominant relaxation process is charge relaxation from $|e\rangle$ to $|g\rangle$ within the lowest-energy valley manifold. The calculation is then similar to that performed in Ref. 18 for the case of a GaAs triple dot.

Unlike GaAs, however, the crystal structure of unstrained Si has a center of inversion symmetry, which leads to the absence of piezoelectric phonons. The electron-phonon interaction for Si therefore consists only of deformation potential terms. In the presence of strain along the $[001]$ (z') axis, we can write this interaction as⁸²

$$H_{\text{ep}} = \Xi_d \nabla \cdot \mathbf{u} + \Xi_u \frac{\partial u_{z'}}{\partial z'}, \quad (60)$$

where Ξ_d and Ξ_u are the dilation and uniaxial deformation potentials, respectively, and the phonon displacement vector \mathbf{u} is given by

$$\mathbf{u}(\mathbf{r}) = \sum_{\mu, \mathbf{k}} \sqrt{\frac{\hbar}{2\rho_0 V_0 c_\mu k}} \left(a_{\mu, \mathbf{k}} + a_{\mu, -\mathbf{k}}^\dagger \right) e^{i\mathbf{k} \cdot \mathbf{r}} \hat{\mathbf{e}}_{\mu, \mathbf{k}} \quad (61)$$

Here, the operator $a_{\mu, \mathbf{k}}^\dagger$ ($a_{\mu, \mathbf{k}}$) creates (annihilates) an acoustic phonon with wave vector \mathbf{k} , polarization μ [the sum in Eq. (61) is taken over one longitudinal mode ($\mu = l$) and two transverse modes ($\mu = p$)], phonon speed c_μ , energy $\varepsilon_{\text{ph}} = \hbar c_\mu k$, and unit polarization vector $\hat{\mathbf{e}}_{\mu, \mathbf{k}}$, ρ_0 is the mass density of the material, and V_0 is the crystal volume. Evaluating the derivatives in H_{ep} leads to

$$H_{\text{ep}} = i \sum_{\mu, \mathbf{k}} \sqrt{\frac{\hbar}{2\rho_0 V_0 c_\mu k}} (\mathbf{k} \cdot \hat{\mathbf{e}}_{\mu, \mathbf{k}} \Xi_d \quad (62)$$

$$+ k_{z'} \hat{z}' \cdot \hat{\mathbf{e}}_{\mu, \mathbf{k}} \Xi_u) (a_{\mu, \mathbf{k}} + a_{\mu, -\mathbf{k}}^\dagger) M_k, \quad (63)$$

where the factor

$$M_k \equiv \sum_{i,j=1}^3 \sum_{\sigma} \langle i | e^{i\mathbf{k} \cdot \mathbf{r}} | j \rangle c_{i\sigma}^\dagger c_{j\sigma} \quad (64)$$

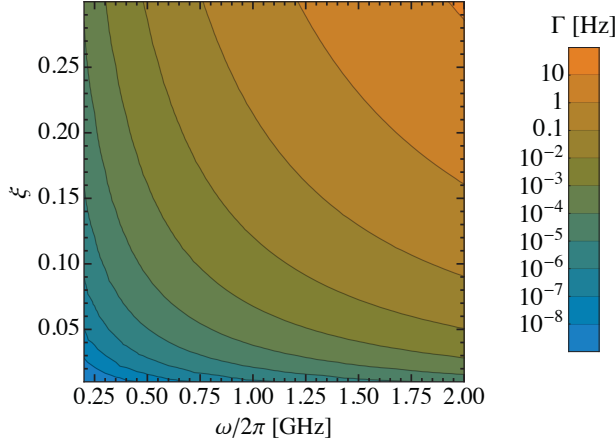


Figure 5. Contour plot of the phonon-induced relaxation rate Γ at the operation point $\epsilon_0 = 0$, as a function of the qubit frequency ω and the charge admixture parameter $\xi = t/\Delta$.

contains the dependence on electronic degrees of freedom and \mathbf{r} is the electron position operator.

The rate Γ of qubit relaxation due to H_{ep} is given by Fermi's golden rule as $\Gamma \sim |\langle g | H_{\text{ep}} | e \rangle|^2 \rho(\omega)$, where $\rho(\omega)$ is the phonon density of states evaluated at the exchange gap ω between the logical qubit states $|g\rangle$ and $|e\rangle$ that determines the energy of the emitted phonon. We can write the relaxation rate as $\Gamma = s_l I_l(\omega/\hbar c_l) + s_p I_p(\omega/\hbar c_p)$, which is expressed in terms of the momentum-space angular integrals

$$I_l(k) \equiv \int (1 + \Lambda \cos^2 \beta)^2 |\langle g | M_k | e \rangle|^2 d\Omega_{\text{ang}}, \quad (65)$$

$$I_p(k) \equiv \int \Lambda^2 \cos^2 \beta \sin^2 \beta |\langle g | M_k | e \rangle|^2 d\Omega_{\text{ang}} \quad (66)$$

and the factors

$$s_\mu = \frac{\omega^3}{8\pi^2 \hbar^4 \rho_0 c_\mu^5} \Xi_d^2, \quad \mu = l, p. \quad (67)$$

In order to obtain Eqs. (65) and (66), we have chosen one of the two transverse ($\mu = p$) polarization axes to lie perpendicular to the direction of uniaxial strain \hat{z}' and defined β as the angle between \mathbf{k} and \hat{z}' . We have also defined the dimensionless parameter $\Lambda \equiv \Xi_u/\Xi_d$ and used Ω_{ang} to denote the momentum-space solid angle.

The relaxation rate at the RX qubit operation point $\epsilon_0 = 0$ is plotted in Fig. 5 as a function of the exchange gap ω and the charge admixture parameter ξ . The parameters used to calculate Γ are the Si transverse effective mass $m^* = 0.19 m_e$, the single-dot size $\sigma = 23$ nm and left-right dot separation $w = 260$ nm,¹⁸ $\rho_0 = 2.33 \times 10^3$ kg/m³, $c_l = 9.33 \times 10^3$ m/s, $c_p = 5.42 \times 10^3$ m/s, $\Xi_d = 5$ eV, and $\Xi_u = 8.77$ eV.⁸³

Comparing Fig. 5 with Fig. 2(e) in Ref. 18 reveals that the rates for phonon-induced relaxation of the resonant exchange qubit in Si are smaller than those for GaAs by several orders of magnitude. For the ranges

of ω and ξ shown in the figure, the relaxation rate is well approximated by $\Gamma = \frac{\omega^5}{\nu_0^4} \xi^4$ with the fit parameter $\nu_0 = 2\pi \times 110$ GHz. We thus find that the relaxation rate for Si exhibits a $\sim \omega^5$ exchange gap dependence, in contrast to the $\sim \omega^3$ dependence for GaAs (see Ref. 18). We note in particular that $\Gamma \lesssim 10$ Hz for all values of ξ and ω shown, which is much smaller than typical values of T_2^{*-1} . Thus, in contrast to GaAs implementations,¹⁸ the coherence time for a RX qubit in a Si triple quantum dot is unlikely to be limited by phonon-induced decay. Si-based RX qubits should therefore enable the strong coupling regime to be achieved for larger ξ^2 , which in principle leads to more rapid and robust entangling gates.

V. PERFORMANCE OF ENTANGLING GATES

Finally, we consider the performance of the two-qubit entangling gates for RX qubits discussed in Sec. III and calculate gate fidelities for each of the three regimes. As we have seen for RX qubits in Si triple quantum dots, the absence of piezoelectric phonons is expected to lead to qubit relaxation times which are much longer than qubit dephasing times (see Sec. IV and Fig. 5). We therefore assume in the present analysis that the dominant decay processes are pure dephasing of the qubits with rates $\gamma_{a,b}$ and the decay of photons out of the resonant cavity with rate κ . Throughout this section, we focus on the strong coupling regime $\gamma_{a,b}, \kappa < g$ of the qubit-resonator interactions and assume that $\omega_0 > \omega_\mu$ for $\mu = a, b$.

A. Dispersive regime

We first consider the dispersive regime, defined by $g_\mu \ll \tilde{\Delta}_\mu = \omega_0 - \omega_\mu$ (see Sec. III A). After making a rotating wave approximation for $\tilde{\Delta}_\mu \ll \omega_0 + \omega_\mu$, the Hamiltonian describing the system is $H_d = H_0 + V$, where H_0 and V are given by Eqs. (15) and (17), respectively. We describe the corresponding time evolution in the presence of qubit dephasing and cavity decay by the master equation^{44,84}

$$\begin{aligned} \dot{\rho}_d = & -i[H_d, \rho_d] + \sum_{\mu=a,b} \frac{\gamma_\mu}{2} (\sigma_\mu^z \rho_d \sigma_\mu^z - \rho_d) \\ & + \frac{\kappa}{2} (2a\rho_d a^\dagger - a^\dagger a \rho_d - \rho_d a^\dagger a), \end{aligned} \quad (68)$$

where ρ_d represents the density matrix of the combined system consisting of both qubits and the resonator. In order to obtain the gate fidelity, we compare the solution of Eq. (68) with that for the ideal evolution (for which $\gamma_{a,b} = \kappa = 0$).

For simplicity, we set $\omega_a = \omega_b \equiv \omega$ (which corresponds to $\tilde{\Delta}_a = \tilde{\Delta}_b \equiv \tilde{\Delta}$), $g_a = g_b \equiv g$, and $\gamma_a = \gamma_b \equiv \gamma$ in what follows. As we consider the dispersive regime of qubit-resonator coupling, we also confine our description

of the resonator mode to the $n = 0$ and $n = 1$ photon subspaces. We can then write

$$h_0 \equiv PH_dP = PH_0P = \frac{\omega}{2}(\sigma_a^z + \sigma_b^z), \quad (69)$$

$$h_1 \equiv QH_dQ = QH_0Q = \omega_0 + \frac{\omega}{2}(\sigma_a^z + \sigma_b^z), \quad (70)$$

$$v \equiv PH_dQ = PVQ = g(\sigma_a^+ + \sigma_b^+), \quad (71)$$

where P and Q are the zero-photon and one-photon projectors defined in Sec. (III C). Using these quantities, we can re-express the master equation [Eq. (68)] in terms of the subspace projections $\rho_{00} \equiv P\rho P$, $\rho_{11} \equiv Q\rho Q$, $\rho_{01} \equiv P\rho Q$, and $\rho_{10} = \rho_{01}^\dagger = Q\rho P$ of the density matrix.

To simplify the analysis, we set $\rho_{11} = 0$, which amounts to neglecting the contribution of the quantum jump term $\kappa a \rho a^\dagger$ in Eq. (68) (this approximation is reasonable for $\kappa, g \ll \tilde{\Delta}$). We also assume that the photon coherences decay much more rapidly than the photon populations and neglect the time evolution of the photon coherences by setting $\dot{\rho}_{01} = 0$. Note that in the absence of decay, setting this condition is equivalent to carrying out perturbation theory for the zero-photon subspace. From Eq. (68), we then find

$$\begin{aligned} \dot{\rho}_{00} = & -i([h_0, \rho_{00}] + v\rho_{01}^\dagger - \rho_{01}v^\dagger) \\ & + \frac{\gamma}{2} \sum_{\mu=a,b} (\sigma_\mu^z \rho_{00} \sigma_\mu^z - \rho_{00}), \end{aligned} \quad (72)$$

$$\begin{aligned} \dot{\rho}_{01} = & -i(h_0\rho_{01} - \rho_{01}h_1 - \rho_{00}v) \\ & + \frac{\gamma}{2} \sum_{\mu=a,b} (\sigma_\mu^z \rho_{01} \sigma_\mu^z - \rho_{01}) - \frac{\kappa}{2} \rho_{01}. \end{aligned} \quad (73)$$

Performing a mapping to a Liouville-space representation [i.e., expressing the density matrix projections as vectors and the superoperator terms in Eqs. (72) and (73) as matrices] and setting $\dot{\rho}_{01} = 0$ enables ρ_{01} to be expressed in terms of ρ_{00} . Solving Eq. (72) with this relation substituted for ρ_{01} then yields an analytical solution for the density matrix $\rho_{00}(\tau)$ as a function of time τ .

In order to calculate the gate fidelity, we choose as the initial state of the system

$$\rho_{00}(0) = |e, g, 0\rangle \langle e, g, 0|. \quad (74)$$

For the ideal evolution, described by setting $\gamma = \kappa = 0$ in Eq. (68), we find

$$\rho_{00,\text{id}}(\tau) \equiv U_d(\tau) \rho_{00}(0) U_d^\dagger(\tau), \quad (75)$$

where $U_d(\tau)$ is given by Eq. (27) with $g_a = g_b = g$, which corresponds to the *i*SWAP gate at the times

$$\tau_n = (4n+1) \frac{\pi \tilde{\Delta}}{2g^2}, \quad n = 0, 1, 2, \dots \quad (76)$$

We calculate the *i*SWAP gate fidelity via

$$F_d(\tau_n) \equiv \text{Tr}[\rho_{00,\text{id}}(\tau_n) \rho_{00}(\tau_n)] \quad (77)$$

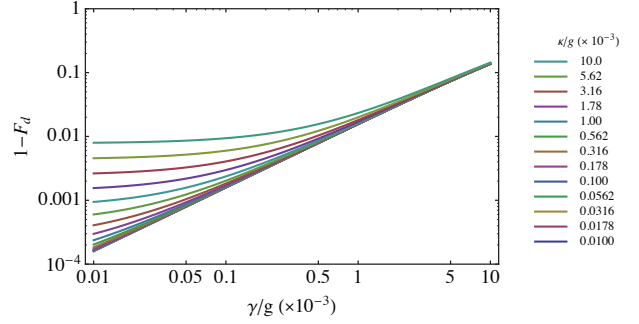


Figure 6. Fidelity $F_d(\tau_0)$ of the *i*SWAP gate as a function of the qubit decay rate γ for several values of the photon decay rate κ , with both rates expressed in units of the coupling strength g . The fidelity is calculated using Eq. (77) for $\tilde{\Delta}/g = 20$.

for the initial state in Eq. (74). The gate error $1 - F_d$ for $\tilde{\Delta}/g = 20$ and $n = 0$ (i.e., at time $\tau_0 = \pi \tilde{\Delta}/2g^2 = 10\pi/g$) is shown in Fig. 6 as a function of γ/g and κ/g , where the chosen ranges of decay rates lie well within the strong coupling regime described by $\gamma/g < 1$ and $\kappa/g < 1$. We see that the error depends more sensitively on γ/g than on κ/g , as is expected for the dispersive regime of RX qubit-resonator coupling. For $g = 2\pi \times 9$ MHz and $\omega_0 = 2\pi \times 1.5$ GHz (see Sec. II), the chosen parameter values correspond to $\omega = 2\pi \times 1.3$ GHz and the *i*SWAP gate time $\tau_0 = 540$ ns, while gate fidelities greater than 0.99 are expected for $\gamma \lesssim 2\pi \times 0.9$ kHz (or $T_2^* \gtrsim 170 \mu\text{s}$) and $\kappa \lesssim 2\pi \times 90$ kHz (or $Q \gtrsim 1.6 \times 10^4$). These upper bounds on γ and κ are consistent with the expectation that gate fidelities for the dispersive regime are limited more by γ than by κ and suggest higher fidelities for systems in which the qubit coherence time is much longer than the resonator photon coherence time. Finally, we note that a controlled-NOT (CNOT) entangling gate can be constructed using two *i*SWAP gates combined with single-qubit rotations.⁷² As all single-qubit rotations for RX qubits can be generated via exchange^{17,18} and $\tau_0 \gg \omega^{-1} \sim 1$ ns (see Sec. IIIB), we can estimate the total CNOT gate time as $\tau_{\text{CNOT}} \sim 2\tau_0 \sim 1 \mu\text{s}$.

B. Driven resonant regime

We now consider the driven resonant regime discussed in Sec. IIIB, in which two RX qubits are entangled through sideband transitions generated by a combination of microwave driving of the resonator and the individual qubit-resonator interactions. As the sideband transitions represent the main entangling mechanism involved in the multi-gate sequence for the controlled-Z gate given in Eq. (45), we focus on a single sideband transition in order to obtain insight into the dependence of the entangling gate fidelity on the qubit and photon decay rates for the driven resonant regime. We therefore estimate the fidelity of a sideband π pulse for one RX qubit coupled to the funda-

mental mode of the resonator.

In order to describe the dynamics in the presence of qubit dephasing and cavity decay with rates γ and κ , respectively, we begin with the master equation

$$\begin{aligned}\dot{\rho}_r = & -i[H_r, \rho_r] + \frac{\gamma}{2}(\sigma^z \rho_r \sigma^z - \rho_r) \\ & + \frac{\kappa}{2}(2\tilde{a}\rho_r\tilde{a}^\dagger - \tilde{a}^\dagger\tilde{a}\rho_r - \rho_r\tilde{a}^\dagger\tilde{a}),\end{aligned}\quad (78)$$

with H_r given in Eq. (28). As in Eq. (29), we apply a displacement transformation $D(\alpha') \equiv e^{\alpha'\tilde{a}^\dagger - \alpha'^*\tilde{a}}$ in order to eliminate the direct action of the drive on the resonator, where $\alpha'(t) = -\varepsilon e^{-i(\nu\tau + \phi)} / (\Delta_0 - i\kappa/2)$ is the steady-state solution of $\dot{\alpha}' + (i\omega_0 + \kappa/2)\alpha' + i\varepsilon e^{-i(\nu\tau + \phi)} = 0$ and $\Delta_0 \equiv \omega_0 - \nu$. Defining $\rho'_r \equiv D^\dagger(\alpha')\rho_r D(\alpha')$, we find

$$\begin{aligned}\dot{\rho}'_r = & -i[H'_r, \rho'_r] + \frac{\gamma}{2}(\sigma^z \rho'_r \sigma^z - \rho'_r) \\ & + \frac{\kappa}{2}(2\tilde{a}\rho'_r\tilde{a}^\dagger - \tilde{a}^\dagger\tilde{a}\rho'_r - \rho'_r\tilde{a}^\dagger\tilde{a}),\end{aligned}\quad (79)$$

where

$$H'_r = \omega_0\tilde{a}^\dagger\tilde{a} + \frac{\omega}{2}\sigma^z + g\sigma^x (\tilde{a}^\dagger + \tilde{a}) - 2\Omega' \cos(\nu\tau) \sigma^x. \quad (80)$$

Here, the Rabi frequency is given by

$$2\Omega' \equiv \frac{2g\varepsilon}{\sqrt{\Delta_0^2 + \kappa^2/4}}, \quad (81)$$

where we include the phase ϕ of the driving field in the definition of Ω' and set $\tan \phi = \kappa/2\Delta_0$, such that Ω' is real even for $\kappa \neq 0$.

We now transform the master equation to the frame rotating at the drive frequency ν . By applying Eq. (31) to the density matrix such that $\rho_r^{\text{rf}} \equiv U_1^\dagger \rho'_r U_1$ and setting $\nu = \omega$, we can rewrite Eq. (79) as

$$\begin{aligned}\dot{\rho}_r^{\text{rf}} = & -i[H_r^{\text{rf}}, \rho_r^{\text{rf}}] + \frac{\gamma}{2}(\sigma^z \rho_r^{\text{rf}} \sigma^z - \rho_r^{\text{rf}}) \\ & + \frac{\kappa}{2}(2\tilde{a}\rho_r^{\text{rf}}\tilde{a}^\dagger - \tilde{a}^\dagger\tilde{a}\rho_r^{\text{rf}} - \rho_r^{\text{rf}}\tilde{a}^\dagger\tilde{a}),\end{aligned}\quad (82)$$

where

$$H_r^{\text{rf}} = \Delta_0\tilde{a}^\dagger\tilde{a} + g(\sigma^+\tilde{a} + \sigma^-\tilde{a}^\dagger) - \Omega'\sigma^x \quad (83)$$

and we have again dropped rapidly oscillating terms $\sim e^{\pm 2i\nu\tau}$ as in Eq. (32). Finally, applying the rotations $\tilde{U}_{\text{rot}} = e^{-i(\pi/4)\sigma^z}$ and U'_{rot} [Eq. (37)] successively such that $\tilde{\rho}_r^{\text{rot}} \equiv U_{\text{rot}}^\dagger \tilde{U}_{\text{rot}}^\dagger \rho_r^{\text{rf}} \tilde{U}_{\text{rot}} U'_{\text{rot}}$ and letting $a \equiv i\tilde{a}$ leads to

$$\begin{aligned}\dot{\tilde{\rho}}_r^{\text{rot}} = & -i[\tilde{H}_r^{\text{rot}}, \tilde{\rho}_r^{\text{rot}}] + \frac{\gamma}{2}(\sigma^y \tilde{\rho}_r^{\text{rot}} \sigma^y - \tilde{\rho}_r^{\text{rot}}) \\ & + \frac{\kappa}{2}(2a\tilde{\rho}_r^{\text{rot}}a^\dagger - a^\dagger a\tilde{\rho}_r^{\text{rot}} - \tilde{\rho}_r^{\text{rot}}a^\dagger a),\end{aligned}\quad (84)$$

where

$$\begin{aligned}\tilde{H}_r^{\text{rot}} = & \Delta_0 a^\dagger a + \Omega'\sigma^z + \frac{g}{2}(\sigma^+ a + \sigma^- a^\dagger + \sigma^+ a^\dagger + \sigma^- a) \\ & + i\frac{g}{2}\sigma^z(a - a^\dagger).\end{aligned}\quad (85)$$

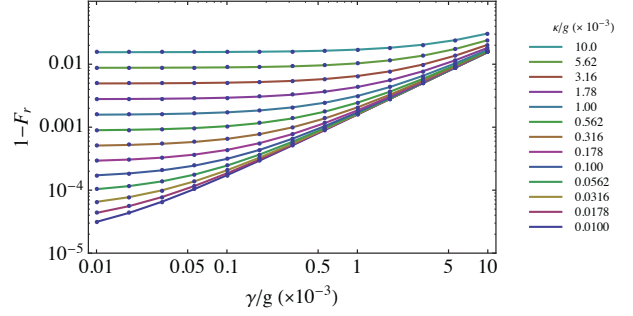


Figure 7. Fidelity $F_r(\tau_\pi)$ of the evolution generated by \tilde{H}_r^{rot} for $\tau_\pi = \pi/g$, corresponding approximately to a sideband π pulse, as a function of the qubit and photon decay rates γ and κ , respectively, in units of the coupling strength g , calculated using Eq. (88) for $\Delta_0/g = 20$. Lines are guides for the eye.

For $\Delta_0 = 2\Omega'$, the time evolution generated by \tilde{H}_r^{rot} closely approximates the sideband transitions obtained in the doubly rotating frame [compare the third term in Eq. (85) with Eqs. (39) and (40)], as we describe below. For simplicity, we therefore calculate the fidelity with respect to the ideal density matrix evolution generated by Eq. (85).

Confining our description to the resonator photon subspaces with $n = 0, 1, 2$, we choose the initial qubit-resonator state

$$\tilde{\rho}_r^{\text{rot}}(0) = |e, 0\rangle\langle e, 0|. \quad (86)$$

The ideal final state generated by a red sideband π pulse $S^-(\pi, 0)$ [see (41)] is then given by

$$\begin{aligned}\rho_\pi \equiv & S^-(\pi, 0) \tilde{\rho}_r^{\text{rot}}(0) S^{-\dagger}(\pi, 0) \\ = & |g, 1\rangle\langle g, 1|\end{aligned}\quad (87)$$

Comparing this state with the final state $\tilde{\rho}_r^{\text{rot, id}}(\tau_\pi)$ after ideal evolution for a time $\tau_\pi = \pi/g$ under the Hamiltonian in Eq. (85) with $\Delta_0 = 2\Omega'$ yields $\text{Tr}[\rho_\pi \tilde{\rho}_r^{\text{rot, id}}(\tau_\pi)] \approx 0.996$. Thus, the ideal evolution generated by \tilde{H}_r^{rot} can itself be regarded approximately as the red sideband transition $S^-(\pi, 0)$.

We numerically calculate the fidelity

$$F_r(\tau_\pi) \equiv \text{Tr}[\tilde{\rho}_r^{\text{rot, id}}(\tau_\pi) \tilde{\rho}_r^{\text{rot}}(\tau_\pi)] \quad (88)$$

as a function of γ/g and κ/g . Fig. 7 shows the corresponding error $1 - F_r$ for $\Delta_0/g = 20$. We see that, compared to the *i*SWAP gate in the dispersive regime (Fig. 6), the fidelity for the sideband π pulse in the driven resonant regime depends more sensitively on the photon decay rate κ/g , while the maximum error is approximately one order of magnitude smaller over the same range of γ/g and κ/g . The parameter values $\Delta_0/g = 20$, $g = 2\pi \times 9$ MHz, and $\omega_0 = 2\pi \times 1.5$ GHz lead to $\omega = 2\pi \times 1.3$ GHz and the gate time $\tau_\pi = 54$ ns, which is a factor of ten shorter than the *i*SWAP gate time τ_0 found in Sec. V A. From Fig. 7, gate fidelities greater than

0.99 are expected for $\gamma \lesssim 2\pi \times 9$ kHz (or $T_2^* \gtrsim 17$ μ s) and $\kappa \lesssim 2\pi \times 51$ kHz (or $Q \gtrsim 2.9 \times 10^4$). Note that the minimum value of T_2^* is also reduced by a factor of ten compared to that for the dispersive regime found in Sec. V A, suggesting that (provided resonators with sufficiently high quality factors are available) sideband-based entangling gates in the driven resonant regime may prove more advantageous for implementations. In addition, an estimate of the controlled-Z gate time based on the five sideband pulses appearing in Eq. (45) yields $\tau_{CZ} \sim 5\pi/g \approx 270$ μ s. As in the previous section, we again neglect the rapid single-qubit exchange rotations (see also Sec. III B), which also serve to convert between the controlled-Z and CNOT gates. Thus, although a controlled-Z gate in the driven resonant regime requires more sideband pulses compared to the two i SWAP gates needed for a CNOT gate in the dispersive regime, we nevertheless find that the total gate time $\tau_{CZ} \ll \tau_{CNOT}$.

C. Driven dispersive regime

Finally, we consider the gate fidelity for the driven dispersive regime (Sec. III C), in which both RX qubits are again coupled to the resonator in the dispersive regime (see Sec. V A), but with $\omega_a \neq \omega_b$ and a microwave driving field applied to the resonator [see Sec. V B and the last term of Eq. (28)]. The master equation in the presence of qubit and cavity decay has the form

$$\begin{aligned} \dot{\rho}_{dd} = & -i[H_{dd}, \rho_{dd}] + \sum_{\mu=a,b} \frac{\gamma_\mu}{2} (\sigma_\mu^z \rho_{dd} \sigma_\mu^z - \rho_{dd}) \\ & + \frac{\kappa}{2} (2a\rho_{dd}a^\dagger - a^\dagger a \rho_{dd} - \rho_{dd} a^\dagger a), \end{aligned} \quad (89)$$

where H_{dd} is given in Eq. (46). As in Sec. V B and Eq. (47), we eliminate the direct action of the driving field on the resonator via a displacement transformation $D(\alpha') \equiv e^{\alpha' a^\dagger - \alpha'^* a}$. Re-expressing the master equation [Eq. (89)] in terms of $\rho'_{dd} \equiv D^\dagger(\alpha') \rho_{dd} D(\alpha')$ leads to

$$\begin{aligned} \dot{\rho}'_{dd} = & -i[H''_{dd}, \rho'_{dd}] + \sum_{\mu=a,b} \frac{\gamma_\mu}{2} (\sigma_\mu^z \rho'_{dd} \sigma_\mu^z - \rho'_{dd}) \\ & + \frac{\kappa}{2} (2a\rho'_{dd}a^\dagger - a^\dagger a \rho'_{dd} - \rho'_{dd} a^\dagger a), \end{aligned} \quad (90)$$

where

$$\begin{aligned} H''_{dd} = & \omega_0 a^\dagger a + \sum_{\mu=a,b} \frac{\omega_\mu}{2} \sigma_\mu^z + \sum_{\mu=a,b} g_\mu \sigma_\mu^x (a + a^\dagger) \\ & - \sum_{\mu=a,b} 2\Omega'_\mu \cos(\nu t) \sigma_\mu^x \end{aligned} \quad (91)$$

with

$$2\Omega'_\mu = \frac{2g_\mu \varepsilon}{\sqrt{\Delta_0^2 + \kappa^2/4}}. \quad (92)$$

As in Eq. (81), we include the phase ϕ in the Rabi frequencies and choose ϕ to satisfy $\tan \phi = \kappa/2\Delta_0$ such that Ω'_μ is real for $\mu = a, b$.

Transforming the master equation to a rotating frame via Eq. (48), defining $\rho_{dd}^{\text{rf}} \equiv U_1^\dagger \rho'_{dd} U_1$, assuming that qubit a is driven resonantly such that $\nu = \omega_a$, and setting $\Omega'_b = 0$ (see Sec. III C) gives

$$\begin{aligned} \dot{\rho}_{dd}^{\text{rf}} = & -i[H_{dd}^{\text{rf}}, \rho_{dd}^{\text{rf}}] + \sum_{\mu=a,b} \frac{\gamma_\mu}{2} (\sigma_\mu^z \rho_{dd}^{\text{rf}} \sigma_\mu^z - \rho_{dd}^{\text{rf}}) \\ & + \frac{\kappa}{2} (2a\rho_{dd}^{\text{rf}}a^\dagger - a^\dagger a \rho_{dd}^{\text{rf}} - \rho_{dd}^{\text{rf}} a^\dagger a), \end{aligned} \quad (93)$$

where

$$H_{dd}^{\text{rf}} = \Delta_0 a^\dagger a - \Omega'_a \sigma_a^x + \frac{\delta}{2} \sigma_b^z + \sum_{\mu=a,b} g_\mu (\sigma_\mu^+ a + \sigma_\mu^- a^\dagger), \quad (94)$$

and rapidly oscillating terms $\sim e^{\pm 2i\nu\tau}$ have been dropped. Finally, applying the rotation in Eq. (50) leads to

$$\begin{aligned} \dot{\rho}_{dd}^{\text{rot}} = & -i[H_{dd}^{\text{rot}}, \rho_{dd}^{\text{rot}}] + \frac{\gamma_a}{2} (\sigma_a^x \rho_{dd}^{\text{rot}} \sigma_a^x - \rho_{dd}^{\text{rot}}) \\ & + \frac{\gamma_b}{2} (\sigma_b^z \rho_{dd}^{\text{rot}} \sigma_b^z - \rho_{dd}^{\text{rot}}) \\ & + \frac{\kappa}{2} (2a\rho_{dd}^{\text{rot}}a^\dagger - a^\dagger a \rho_{dd}^{\text{rot}} - \rho_{dd}^{\text{rot}} a^\dagger a), \end{aligned} \quad (95)$$

where $H_{dd}^{\text{rot}} = H''_0 + V_{dd}$, with

$$H''_0 = \Delta_0 a^\dagger a + \Omega'_a \sigma_a^z + \frac{\delta}{2} \sigma_b^z \quad (96)$$

and V_{dd} given by Eq. (52).

We now follow an approach similar to that used for the dispersive regime in Sec. V A in order to numerically calculate the fidelity using Eq. (95). Confining the description to the $n = 0$ and $n = 1$ subspaces, we find the subspace projections of H_{dd}^{rot}

$$h'_0 \equiv P H_{dd}^{\text{rot}} P = P H''_0 P = \Omega'_a \sigma_a^z + \frac{\delta}{2} \sigma_b^z, \quad (97)$$

$$h'_1 \equiv Q H_{dd}^{\text{rot}} Q = Q H''_0 Q = \Delta_0 + \Omega'_a \sigma_a^z + \frac{\delta}{2} \sigma_b^z, \quad (98)$$

$$v' \equiv P H_{dd}^{\text{rot}} Q = P V_{dd} Q = \frac{g_a}{2} (-\sigma_a^z + i\sigma_a^y) + g_b \sigma_b^+. \quad (99)$$

In terms of the associated subspace projections of the density matrix $\rho'_{00} \equiv P \rho_{dd}^{\text{rot}} P$, $\rho'_{01} \equiv P \rho_{dd}^{\text{rot}} Q$ and $\rho'_{11} = 0$ (see Sec. V A), Eq. (95) yields

$$\begin{aligned} \dot{\rho}'_{00} = & -i([h'_0, \rho'_{00}] + v' \rho'_{01} - \rho'_{01} v') \\ & + \frac{\gamma_a}{2} (\sigma_a^x \rho'_{00} \sigma_a^x - \rho'_{00}) + \frac{\gamma_b}{2} (\sigma_b^z \rho'_{00} \sigma_b^z - \rho'_{00}), \end{aligned} \quad (100)$$

$$\begin{aligned} \dot{\rho}'_{01} = & -i(h'_0 \rho'_{01} - \rho'_{01} h'_1 - \rho'_{00} v') \\ & + \frac{\gamma_a}{2} (\sigma_a^x \rho'_{01} \sigma_a^x - \rho'_{01}) + \frac{\gamma_b}{2} (\sigma_b^z \rho'_{01} \sigma_b^z - \rho'_{01}) \\ & - \frac{\kappa}{2} \rho'_{01}. \end{aligned} \quad (101)$$

As described in Sec. V A, we set $\rho'_{01} = 0$ and apply a Liouville-space mapping in order to solve for $\rho'_{00}(\tau)$.

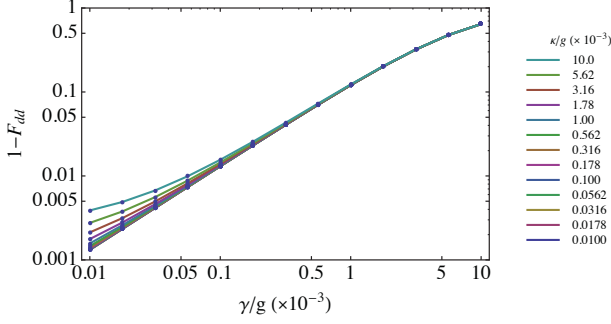


Figure 8. Fidelity $F_{dd}(\tau_0)$ of the evolution generated by $H_{dd}^{\text{rot}'}$ as a function of the qubit and photon decay rates γ and κ , respectively, in units of the coupling strength g , calculated using Eq. (8) for $\Delta_0/g = 20$ and $\delta/g = 4$. Lines are guides for the eye.

In Sec. III C, we showed that the i SWAP entangling gate can be generated by the interaction in a doubly rotating frame for $2\tilde{\Omega}_a = \delta$ [see Eq. (59)]. Setting $2\Omega'_a = \delta$, we incorporate this condition into the present analysis via Eq. (58). We again take $\rho_{00}(0)$ [Eq. (74)] as the initial state of the system and obtain $\rho'_{00}(\tau)$ numerically. Defining $g \equiv g_a$, setting $\Delta_0/g = 20$, and choosing the i SWAP gate time

$$\begin{aligned} \tau_0 &= \pi \frac{\Delta_0 - \delta}{2g^2} \sqrt{\frac{2(\Delta_0 + \delta)}{\delta}} \\ &= 32\sqrt{3} \frac{\pi}{g}, \end{aligned} \quad (102)$$

we find $\text{Tr}[\rho_{00,\text{id}}(\tau_0)\rho'_{00,\text{id}}(\tau_0)] \approx 0.999$, indicating that the evolution generated by $H_{dd}^{\text{rot}'}$ for $2\Omega'_a = \delta$ and the constraint in Eq. (58) closely matches an ideal i SWAP gate. Thus, we approximate the i SWAP gate fidelity for the driven dispersive regime by

$$F_{dd}(\tau_0) \equiv \text{Tr}[\rho'_{00,\text{id}}(\tau_0)\rho'_{00}(\tau_0)]. \quad (103)$$

Figure 8 shows the error $1 - F_{dd}$ as a function of the qubit and cavity decay rates γ/g and κ/g for $\Delta_0/g = 20$ and $\delta/g = 4$. We note that, as in the dispersive regime considered in Sec. V A, the error depends more sensitively on γ/g than κ/g and is also larger than that for the driven resonant regime. For $\Delta_0/g = 20$, $g = 2\pi \times 9$ MHz, and $\omega_0 = 2\pi \times 1.5$ GHz, we find $\omega = 2\pi \times 1.3$ GHz and the i SWAP gate time $\tau_0 = 3.0 \mu\text{s}$. Gate fidelities greater than 0.99 correspond to $\gamma \lesssim 2\pi \times 0.51$ kHz (or $T_2^* \gtrsim 310 \mu\text{s}$) and $\kappa \lesssim 2\pi \times 90$ kHz (or $Q \gtrsim 1.6 \times 10^4$). While the longer gate time τ_0 relative to that chosen in Sec. V A leads to a longer minimum T_2^* , we again find that the gate fidelity should be higher for systems in which the coherence time of the qubit is much longer than that of the resonator photons, as is expected for the dispersive regime. Finally, we use the approach described in Sec. V A to estimate the total CNOT gate time as $\tau_{\text{CNOT}} \sim 2\tau_0 \sim 6 \mu\text{s}$ and thus again find that $\tau_{\text{CZ}} \ll \tau_{\text{CNOT}}$ (see Sec. V B).

VI. CONCLUSIONS

In the present work, we have analyzed three approaches drawn from a combination of circuit QED and Hartmann-Hahn double resonance techniques for entangling spatially separated RX qubits via a superconducting transmission line resonator. We derived both the form of the RX qubit-resonator coupling and resonator-mediated entangling gates in the dispersive, driven resonant, and driven dispersive regimes. While both dispersive regimes yield two-qubit gate rates $\sim \xi^4$, where $\xi \equiv t/\Delta$ is the charge admixture parameter for the RX qubit and is related to the qubit-resonator coupling strength via $g \sim \xi^2$, rapid gates with rates $\sim \xi^2$ and smaller error are possible in the driven resonant regime.

Our results show that an implementation of RX qubits in silicon triple quantum dots in principle enables robustness to phonon-induced relaxation and possesses characteristics highly favorable for achieving the strong coupling regime of interaction with the resonator. Furthermore, the analysis of gate fidelities for the three regimes we consider suggests that, while the requirements for resonator quality factors are somewhat relaxed in the dispersive regimes, high-fidelity entangling gates based on sideband transitions in the driven resonant regime in combination with rapid ($\tau_{\text{gate}} \sim \omega^{-1} \lesssim 1$ ns) single-qubit rotations via exchange may prove advantageous for implementations with resonators of sufficiently high quality factors. In particular, although five sideband pulses are required to construct a controlled-Z gate according to Eq. (45), we expect that the total gate time should still be considerably shorter than those for controlled-NOT gates carried out using two i SWAP gates in the dispersive and driven dispersive regimes. We therefore find that the exchange-based universal control intrinsic to RX qubits enables rapid entangling gates in the driven resonant regime.

Many potential future directions remain to be explored. Experiments will ultimately provide more insight into the achievable coherence times, resonator quality factors, and optimal coupling regime for entanglement within the RX qubit-resonator system. Identifying methods for integrating this basic unit into a robust modular architecture also remains an open challenge. Additionally, while the focus of the present work is on so-called transverse RX qubit-resonator dipole coupling of the form $\sigma_x(a + a^\dagger)$, future work may involve investigating potential improvements in the performance of entangling gates for RX qubits via longitudinal dipole coupling of the form $\sigma_z(a + a^\dagger)$.^{57,85} Finally, the implementation of RX qubits in silicon will provide an opportunity to verify the expected improvements in coherence compared to RX qubits in GaAs.

ACKNOWLEDGMENTS

We thank B. E. Kane and F. W. Strauch for helpful discussions.

* vsriniv@umd.edu

- ¹ D. P. DiVincenzo, Fortschr. Phys. **48**, 771 (2000).
- ² T. D. Ladd, F. Jelezko, R. Laflamme, Y. Nakamura, C. Monroe, and J. L. O'Brien, Nature **464**, 45 (2010).
- ³ D. D. Awschalom, L. C. Bassett, A. S. Dzurak, E. L. Hu, and J. R. Petta, Science **339**, 1174 (2013).
- ⁴ D. Loss and D. P. DiVincenzo, Phys. Rev. A **57**, 120 (1998).
- ⁵ J. M. Taylor, H. A. Engel, W. Dur, A. Yacoby, C. M. Marcus, P. Zoller, and M. D. Lukin, Nature Phys. **1**, 177 (2005).
- ⁶ R. Hanson, L. P. Kouwenhoven, J. R. Petta, S. Tarucha, and L. M. K. Vandersypen, Rev. Mod. Phys. **79**, 1217 (2007).
- ⁷ F. H. L. Koppens, C. Buizert, K. J. Tielrooij, I. T. Vink, K. C. Nowack, T. Meunier, L. P. Kouwenhoven, and L. M. K. Vandersypen, Nature **442**, 766 (2006).
- ⁸ K. C. Nowack, F. H. L. Koppens, Y. V. Nazarov, and L. M. K. Vandersypen, Science **318**, 1430 (2007).
- ⁹ S. Nadj-Perge, S. M. Frolov, E. P. A. M. Bakkers, and L. P. Kouwenhoven, Nature **468**, 1084 (2010).
- ¹⁰ Y. Tokura, W. G. van der Wiel, T. Obata, and S. Tarucha, Phys. Rev. Lett. **96**, 047202 (2006).
- ¹¹ M. Pioro-Ladriere, T. Obata, Y. Tokura, Y. S. Shin, T. Kubo, K. Yoshida, T. Taniyama, and S. Tarucha, Nature Phys. **4**, 776 (2008).
- ¹² J. Levy, Phys. Rev. Lett. **89**, 147902 (2002).
- ¹³ J. R. Petta, A. C. Johnson, J. M. Taylor, E. A. Laird, A. Yacoby, M. D. Lukin, C. M. Marcus, M. P. Hanson, and A. C. Gossard, Science **309**, 2180 (2005).
- ¹⁴ D. P. DiVincenzo, D. Bacon, J. Kempe, G. Burkard, and K. B. Whaley, Nature **408**, 339 (2000).
- ¹⁵ E. A. Laird, J. M. Taylor, D. P. DiVincenzo, C. M. Marcus, M. P. Hanson, and A. C. Gossard, Phys. Rev. B **82**, 075403 (2010).
- ¹⁶ J. Medford, J. Beil, J. M. Taylor, S. D. Bartlett, A. C. Doherty, E. I. Rashba, D. P. DiVincenzo, H. Lu, A. C. Gossard, and C. M. Marcus, Nature Nano. **8**, 654 (2013).
- ¹⁷ J. Medford, J. Beil, J. M. Taylor, E. I. Rashba, H. Lu, A. C. Gossard, and C. M. Marcus, Phys. Rev. Lett. **111**, 050501 (2013).
- ¹⁸ J. M. Taylor, V. Srinivasa, and J. Medford, Phys. Rev. Lett. **111**, 050502 (2013).
- ¹⁹ D. A. Lidar, D. Bacon, J. Kempe, and K. Birgitta Whaley, Phys. Rev. A **61**, 052307 (2000).
- ²⁰ L. Gaudreau, G. Granger, A. Kam, G. C. Aers, S. A. Studenikin, P. Zawadzki, M. Pioro-Ladriere, Z. R. Wasilewski, and A. S. Sachrajda, Nature Phys. **8**, 54 (2012).
- ²¹ Z. Shi, C. B. Simmons, J. R. Prance, J. K. Gamble, T. S. Koh, Y.-P. Shim, X. Hu, D. E. Savage, M. G. Lagally, M. A. Eriksson, M. Friesen, and S. N. Coppersmith, Phys. Rev. Lett. **108**, 140503 (2012).
- ²² D. Kim, Z. Shi, C. B. Simmons, D. R. Ward, J. R. Prance, T. S. Koh, J. K. Gamble, D. E. Savage, M. G. Lagally, M. Friesen, S. N. Coppersmith, and M. A. Eriksson, Nature **511**, 70 (2014).
- ²³ K. Eng, T. D. Ladd, A. Smith, M. G. Borselli, A. A. Kiselev, B. H. Fong, K. S. Holabird, T. M. Hazard, B. Huang, P. W. Deelman, *et al.*, Sci. Adv. **1**, e1500214 (2015).
- ²⁴ J. Fei, J.-T. Hung, T. S. Koh, Y.-P. Shim, S. N. Coppersmith, X. Hu, and M. Friesen, Phys. Rev. B **91**, 205434 (2015).
- ²⁵ M. Russ and G. Burkard, Phys. Rev. B **91**, 235411 (2015).
- ²⁶ Y. P. Shim and C. Tahan, arXiv:1602.00320 (2016).
- ²⁷ J. Koch, T. M. Yu, J. Gambetta, A. A. Houck, D. I. Schuster, J. Majer, A. Blais, M. H. Devoret, S. M. Girvin, and R. J. Schoelkopf, Phys. Rev. A **76**, 042319 (2007).
- ²⁸ A. A. Houck, J. Koch, M. H. Devoret, S. M. Girvin, and R. J. Schoelkopf, Quantum Inf. Process. **8**, 105 (2009).
- ²⁹ F. Meier, J. Levy, and D. Loss, Phys. Rev. Lett. **90**, 047901 (2003).
- ³⁰ F. Meier, J. Levy, and D. Loss, Phys. Rev. B **68**, 134417 (2003).
- ³¹ V. Srinivasa and J. Levy, Phys. Rev. B **80**, 024414 (2009).
- ³² B. H. Fong and S. M. Wandzura, Quantum Inf. Comput. **11**, 1003 (2011).
- ³³ A. C. Doherty and M. P. Wardrop, Phys. Rev. Lett. **111**, 050503 (2013).
- ³⁴ G. Burkard, D. Loss, and D. P. DiVincenzo, Phys. Rev. B **59**, 2070 (1999).
- ³⁵ A. Pal, E. I. Rashba, and B. I. Halperin, Phys. Rev. X **4**, 011012 (2014).
- ³⁶ A. Pal, E. I. Rashba, and B. I. Halperin, Phys. Rev. B **92**, 125409 (2015).
- ³⁷ F. Setiawan, H.-Y. Hui, J. P. Kestner, X. Wang, and S. D. Sarma, Phys. Rev. B **89**, 085314 (2014).
- ³⁸ M. Friesen, A. Biswas, X. Hu, and D. Lidar, Phys. Rev. Lett. **98**, 230503 (2007).
- ³⁹ V. Srinivasa, J. Levy, and C. S. Hellberg, Phys. Rev. B **76**, 094411 (2007).
- ⁴⁰ L. Trifunovic, O. Dial, M. Trif, J. R. Wootton, R. Abebe, A. Yacoby, and D. Loss, Phys. Rev. X **2**, 011006 (2012).
- ⁴¹ C. Monroe, R. Raussendorf, A. Ruthven, K. R. Brown, P. Maunz, L.-M. Duan, and J. Kim, Phys. Rev. A **89**, 022317 (2014).
- ⁴² A. Blais, R.-S. Huang, A. Wallraff, S. M. Girvin, and R. J. Schoelkopf, Phys. Rev. A **69**, 062320 (2004).
- ⁴³ A. Wallraff, D. I. Schuster, A. Blais, L. Frunzio, R. S. Huang, J. Majer, S. Kumar, S. M. Girvin, and R. J. Schoelkopf, Nature **431**, 162 (2004).
- ⁴⁴ A. Blais, J. Gambetta, A. Wallraff, D. I. Schuster, S. M. Girvin, M. H. Devoret, and R. J. Schoelkopf, Phys. Rev. A **75**, 032329 (2007).
- ⁴⁵ J. Majer, J. M. Chow, J. M. Gambetta, J. Koch, B. R. Johnson, J. A. Schreier, L. Frunzio, D. I. Schuster, A. A. Houck, A. Wallraff, A. Blais, M. H. Devoret, S. M. Girvin, and R. J. Schoelkopf, Nature **449**, 443 (2007).
- ⁴⁶ M. A. Sillanpää, J. I. Park, and R. W. Simmonds, Nature **449**, 438 (2007).
- ⁴⁷ L. DiCarlo, J. M. Chow, J. M. Gambetta, L. S. Bishop,

- B. R. Johnson, D. I. Schuster, J. Majer, A. Blais, L. Frunzio, S. M. Girvin, and R. J. Schoelkopf, *Nature* **460**, 240 (2009).
- ⁴⁸ L. DiCarlo, M. D. Reed, L. Sun, B. R. Johnson, J. M. Chow, J. M. Gambetta, L. Frunzio, S. M. Girvin, M. H. Devoret, and R. J. Schoelkopf, *Nature* **467**, 574 (2010).
- ⁴⁹ L. Childress, A. S. Sørensen, and M. D. Lukin, *Phys. Rev. A* **69**, 042302 (2004).
- ⁵⁰ T. Frey, P. J. Leek, M. Beck, A. Blais, T. Ihn, K. Ensslin, and A. Wallraff, *Phys. Rev. Lett.* **108**, 046807 (2012).
- ⁵¹ M. R. Delbecq, L. E. Bruhat, J. J. Viennot, S. Datta, A. Cottet, and T. Kontos, *Nat. Commun.* **4**, 1400 (2013).
- ⁵² H. Toida, T. Nakajima, and S. Komiyama, *Phys. Rev. Lett.* **110**, 066802 (2013).
- ⁵³ Y.-Y. Liu, J. Stehlik, C. Eichler, M. J. Gullans, J. M. Taylor, and J. R. Petta, *Science* **347**, 285 (2015).
- ⁵⁴ M. J. Gullans, Y.-Y. Liu, J. Stehlik, J. R. Petta, and J. M. Taylor, *Phys. Rev. Lett.* **114**, 196802 (2015).
- ⁵⁵ G. Burkard and A. Imamoglu, *Phys. Rev. B* **74**, 041307 (2006).
- ⁵⁶ J. M. Taylor and M. D. Lukin, *arXiv:cond-mat/0605144* (2006).
- ⁵⁷ P.-Q. Jin, M. Marthaler, A. Shnirman, and G. Schön, *Physical Review Letters* **108**, 190506 (2012).
- ⁵⁸ X. Hu, Y.-x. Liu, and F. Nori, *Phys. Rev. B* **86**, 035314 (2012).
- ⁵⁹ K. D. Petersson, L. W. McFaul, M. D. Schroer, M. Jung, J. M. Taylor, A. A. Houck, and J. R. Petta, *Nature* **490**, 380 (2012).
- ⁶⁰ G. Tosi, F. A. Mohiyaddin, H. Huebl, and A. Morello, *AIP Advances* **4**, (2014).
- ⁶¹ G. Tosi, F. Mohiyaddin, S. Tenberg, R. Rahman, G. Klimeck, and A. Morello, *arXiv:1509.08538* (2015).
- ⁶² F. A. Zwanenburg, A. S. Dzurak, A. Morello, M. Y. Simmons, L. C. L. Hollenberg, G. Klimeck, S. Rogge, S. N. Coppersmith, and M. A. Eriksson, *Rev. Mod. Phys.* **85**, 961 (2013).
- ⁶³ E. Kawakami, P. Scarlino, D. R. Ward, F. R. Braakman, D. E. Savage, M. G. Lagally, M. Friesen, S. N. Coppersmith, M. A. Eriksson, and L. M. K. Vandersypen, *Nat. Nanotechnol.* **9**, 666 (2014).
- ⁶⁴ J. T. Muhonen, J. P. Dehollain, A. Laucht, F. E. Hudson, R. Kalra, T. Sekiguchi, K. M. Itoh, D. N. Jamieson, J. C. McCallum, A. S. Dzurak, and A. Morello, *Nat. Nanotechnol.* **9**, 986 (2014).
- ⁶⁵ M. Veldhorst, C. H. Yang, J. C. C. Hwang, W. Huang, J. P. Dehollain, J. T. Muhonen, S. Simmons, A. Laucht, F. E. Hudson, K. M. Itoh, A. Morello, and A. S. Dzurak, *Nature* **526**, 410 (2015).
- ⁶⁶ K. Takeda, J. Kamioka, T. Otsuka, J. Yoneda, T. Nakajima, M. R. Delbecq, S. Amaha, G. Allison, T. Koder, S. Oda, and S. Tarucha, *arXiv:1602.07833* (2016).
- ⁶⁷ E. Kawakami, T. Jullien, P. Scarlino, D. R. Ward, D. E. Savage, M. G. Lagally, V. V. Dobrovitski, M. Friesen, S. N. Coppersmith, M. A. Eriksson, and L. M. K. Vandersypen, *arXiv:1602.08334* (2016).
- ⁶⁸ M. Russ and G. Burkard, *Phys. Rev. B* **92**, 205412 (2015).
- ⁶⁹ S. R. Hartmann and E. L. Hahn, *Phys. Rev.* **128**, 2042 (1962).
- ⁷⁰ N. Samkharadze, A. Bruno, P. Scarlino, G. Zheng, D. P. DiVincenzo, L. DiCarlo, and L. M. K. Vandersypen, *arXiv:1511.01760* (2015).
- ⁷¹ P. Meystre and M. Sargent, *Elements of Quantum Optics*, 4th ed. (Springer, 2007).
- ⁷² N. Schuch and J. Siewert, *Phys. Rev. A* **67**, 032301 (2003).
- ⁷³ A. Wallraff, D. I. Schuster, A. Blais, J. M. Gambetta, J. Schreier, L. Frunzio, M. H. Devoret, S. M. Girvin, and R. J. Schoelkopf, *Phys. Rev. Lett.* **99**, 050501 (2007).
- ⁷⁴ P. J. Leek, S. Filipp, P. Maurer, M. Baur, R. Bianchetti, J. M. Fink, M. Göppl, L. Steffen, and A. Wallraff, *Phys. Rev. B* **79**, 180511 (2009).
- ⁷⁵ J. I. Cirac and P. Zoller, *Phys. Rev. Lett.* **74**, 4091 (1995).
- ⁷⁶ A. M. Childs and I. L. Chuang, *Phys. Rev. A* **63**, 012306 (2000).
- ⁷⁷ G. Haack, F. Helmer, M. Mariantoni, F. Marquardt, and E. Solano, *Phys. Rev. B* **82**, 024514 (2010).
- ⁷⁸ H. Kim, T. C. Shen, K. Roy-Choudhury, G. S. Solomon, and E. Waks, *Phys. Rev. Lett.* **113**, 027403 (2014).
- ⁷⁹ B. R. Mollow, *Phys. Rev.* **188**, 1969 (1969).
- ⁸⁰ C. Rigetti, A. Blais, and M. Devoret, *Phys. Rev. Lett.* **94**, 240502 (2005).
- ⁸¹ C. H. Yang, A. Rossi, R. Ruskov, N. S. Lai, F. A. Mohiyaddin, S. Lee, C. Tahan, G. Klimeck, A. Morello, and A. S. Dzurak, *Nat. Commun.* **4** (2013).
- ⁸² P. Yu and M. Cardona, *Fundamentals of Semiconductors: Physics and Materials Properties*, Graduate Texts in Physics (Springer, 2010).
- ⁸³ C. Tahan and R. Joynt, *Phys. Rev. B* **89**, 075302 (2014).
- ⁸⁴ P. Lambropoulos and D. Petrosyan, *Fundamentals of Quantum Optics and Quantum Information* (Springer, 2006).
- ⁸⁵ P. M. Billangeon, J. S. Tsai, and Y. Nakamura, *Phys. Rev. B* **91**, 094517 (2015).